Analysing the stability of premixed rich hydrogen-air flame with the use of two-step models

V.V. Gubernov[a,*], A.V. Kolobov[a], A.A. Polezhaev[a], H.S. Sidhu[b]

[a] *I.E. Tamm Theory Department, P.N. Lebedev Physical Institute of Russian Academy of Sciences, Moscow 119991, 53 Leninskii prosp., Russian Federation*
[b] *School of Physical, Environmental and Mathematical Sciences, University of New South Wales at the Australian Defence Force Academy, Canberra, ACT 2600, Australia*

Abstract

In this paper we investigate the thermal-diffusive instability of premixed adiabatic flames in rich hydrogen-air mixtures at normal ambient conditions. Several models which feature the same two-step global kinetics with chain-branching and recombination reaction steps are considered. These global kinetic steps are assumed to be controlled by different elementary reactions. The flame speed and structure are investigated numerically by using the shooting-relaxation algorithms. The stability is studied by means of the Evans function method and by direct integration of the governing partial differential equations. It is demonstrated that the two-step models are capable of accurately predicting the speed and structure of combustion waves as well as flame stability and frequency of pulsations of unsteady combustion waves.

Keywords: premixed flames, thermal-diffusive instabilities, flammability limit, hydrogen-air combustion

*Corresponding author. Address: P.N. Lebedev Physical Institute of Russian Academy of Sciences, Moscow 119991, 53 Leninskii prosp., Russian Federation, Tel.: +7(499)132-6978, Fax: + 7(499) 135 8533

Email addresses: gubernov@lpi.ru (V.V. Gubernov), kolobov@lpi.ru (A.V. Kolobov), apol@lpi.ru (A.A. Polezhaev), h.sidhu@adfa.edu.au (H.S. Sidhu)

1. Introduction

It is well known that combustion waves can propagate in rich hydrogen-air mixtures only up to certain values of equivalence ratio, beyond which the flame extinguishes. Although many factors may affect the observed flammability limits, such as buoyancy, diffusion, kinetics etc, which may also come into play with each other, it is generally common to focus on certain isolated physical processes while analysing such complex phenomenon in order to reveal their role. In this paper, the consideration is devoted to the thermal-diffusional approximation of the premixed flame propagation. In this frame the flammability limit may be caused by several factors. In the nonadiabatic case the flame can extinguish due to the presence of conductive or radiative heat losses [1, 2]. In the adiabatic limit the explanation of flame extinction can be given as the competition of chain-branching and recombination reactions [3], i.e. the radical quenching, or due to the onset of complex oscillating dynamical regimes [2, 4, 5, 6]. The latter scenario is closely related to the loss of stability of planar flame [6, 5]. Therefore the analysis of flame stability is important for the understanding of combustion wave extinction. Besides the fundamental interest in this subject, finding the flammability limits is also important from the point of view of hydrogen safety. In this paper we focus on the analysis of near-limit behaviour of premixed flames in rich hydrogen-air mixtures at normal ambient conditions ($298K$ and $1atm$).

Although to date there is a good understanding of the hydrogen oxidation chemistry which includes eight chemical species [7, 8], there is still a lack of short reduced mechanisms for modelling the problems with multi time and length scales such as studying the flame stability and time dependent regimes of flame propagation. One of the first models of the H_2 - O_2 mixture combustion was proposed in [9]. This model included the branching $A + B \rightarrow 3B$ and the recombination $B + B + M \rightarrow P + M$ steps, where A is the deficient component concentration, for example, O_2, B is the H atom concentration which is considered as the only radical involved in the reaction. In [10] the steady-state approximation for O, OH and HO_2 was adopted and a similar model was derived and investigated for rich hydrogen-oxygen flames. In this case the rate of the first global reaction is governed by the elementary step $H+O_2 \rightarrow OH+H$ and the rate of the second global reaction is governed by elementary reaction $H + H + M \rightarrow H_2 + M$. In [11] the two-step reaction mechanism was further developed. It was shown to be capable of producing reasonably accurate predictions for the flame structure and

speed as compared to the data obtained from both the detailed chemistry calculations and experiments. The two-step mechanism was used in [12] to study the asymptotic structure of premixed hydrogen-air flames. Recently in [13, 14], the model was tested using numerical calculations with detailed mechanism of the reaction and it was demonstrated that the two-step reaction model gives a good approximation for the velocity of the flame propagation.

As discussed in [13, 14], the rate of H recombination is governed by two elementary reactions $H+H+M \rightarrow H_2+M$ and $H+O_2+M \rightarrow HO_2+M$. The H-radical recombination with O_2 has a higher rate and must be faster in the presence of appreciable oxygen concentration. The square-law termination reaction however, could play a substantial role in the case of hydrogen rich mixtures and/or slow recombination regimes when the concentration of H atoms becomes significant and O_2 is rapidly depleted in the course of fast branching. The importance of the linear recombination reaction of H is also discussed in [3, 15].

In [3, 10, 16, 17] the significance of hydroperoxyl radical is speculated. In [3] it is demonstrated that in rich hydrogen-oxygen flames HO_2 can attain quite significant values and should be taken into consideration, while concentrations of O and OH are still small and corresponding reactions related to them can be neglected. The inclusion of HO_2 radical results in the two-step model introduced by Liñán as reported in [16]. The model was studied in [3], where it is shown to accurately predict the speed and structure of the rich hydrogen-oxygen flames as compared to the calculations based on the detailed reaction mechanism. In [17], the mechanism was further modified to include an initiation reaction $H_2 + O_2 \rightarrow HO_2 + H$ and the equilibrium assumption for hydroperoxyl radical was to relaxed. The resulting model was found to be suitable for analysing deflagration, autoignition and diffusion hydrogen-air flames.

Numerical analysis of the models with detailed reaction mechanisms have been used to study various aspects of premixed hydrogen flames such as comparison with experiments [18], effect of the multicomponent transport [19] etc. In a number of papers [2, 20, 21, 22, 15, 3, 4] the detailed kinetic mechanism was used to numerically investigate the dynamics of premixed hydrogen flame propagation near the rich flammability limit. In [22] it was shown that as the composition of the hydrogen-air mixture gets richer when the oscillatory behaviour is observed. The onset of pulsations was found at the H_2 content of $75 - 76\%$ in the mixture where uncertainty was related to computational error. Qualitatively similar results were obtained in [15].

These authors drew a conclusion that the observed oscillations are the results of underlying physics, and not a "numerical artefact". The emergence of oscillations was attributed to the competition of the chain-branching and termination reactions for the H radicals. The critical hydrogen content was determined to be around 79%. As the equivalence ratio was increased the oscillations of the flame speed became more relaxational. The amplitude and period of oscillations were reported to grow. At certain conditions, period doubling behaviour was clearly observed in the time histories of the flame speed. The increase of hydrogen content to 84% led to flame extinction i.e. neither travelling nor pulsating combustion wave propagation regimes were possible at these rich compositions. This complex dynamical scenario is similar to the observation of flame oscillations in solid combustion, one- and two-step reaction models (see [5] for literature review). In [21] the results summarized above were qualitatively confirmed, although the onset of pulsations was determined for mixtures with more than 75% of H_2. The flammability limit was also reduced to 82% of hydrogen in fresh mixture. In [2, 20], both the case with and without heat loss were studied for normal conditions and elevated pressures. For normal conditions in the adiabatic case the onset of pulsations was found for equivalence ratio near 7.4, at 7.6 the solution of period two was observed, whereas at higher values of equivalence ratio the oscillations become very relaxational, that is the flame exhibits long periods of "depression", when propagation stops, followed by intervals of recovery, when flame speed peaks to maximal values. As the mixture gets richer, the oscillatory route to extinction was observed. In [4] the premixed hydrogen-oxygen flames were found to oscillate as the mixture got richer. These oscillations were attributed to diffusive-thermal instability.

Although there is an apparent progress in the stability analysis of H_2-air flame near the rich flammability limit in terms of numerical modelling with the detailed kinetics, there have been no attempts to investigate the stability problem based on the models with reduced reaction mechanisms. As described above, models with two-step kinetics are capable to predict the flame speed and structure with a reasonable accuracy. Therefore one can expect that such reduced models to be a useful alternative to the computationally expensive calculations based on detailed kinetics in the stability analysis of the hydrogen-air flame and the investigation of complex dynamical regimes such as period doubling and oscillatory route to extinction. From the mathematical point of view, the two-step chain-branching models, the Zeldovich-Liñán model [23, 24] with the quadratic law for the radical recombination and

the Dold model [25] with the linear radical recombination reaction, are the most relevant to the two-step reduced models for hydrogen-air combustion outlined above.

The Zeldovich-Liñán model comprises a chain branching reaction $A+B \rightarrow 2B$, and a chain-breaking (or recombination) reaction $B+B+M \rightarrow 2P+M$, where A is the fuel, B is the intermediate radical, P is the product, and M is a third body of collision needed for recombination, which is not changed by the reaction. It is assumed that the first reaction has a large activation energy and negligible heat of the reaction whereas, the recombination reaction has zero activation energy and is exothermic. The stability analysis for this model was carried out in [26]. The chain-branching models with first-order recombination reactions, $B+M \rightarrow P+M$, have become very popular in the last decade. Partly, this is due to the fact that for the models with first-order reaction, like the model introduced in [25], both the properties and stability of the travelling combustion waves can be studied using the activation energy asymptotic analysis. The properties of premixed combustion waves in this model were investigated in various aspects in a number of papers [5, 25, 27, 28, 29, 30]. As noted in [26], the kinetics can change the properties of combustion waves and the results obtained for the models with linear and quadratic recombination reaction can be significantly different.

The aim of the work presented in the current paper is to investigate the stability of the premixed hydrogen-air flame near the rich flammability limit by using the reduced two-step chain-branching reaction models. We consider three types of models: the model with quadratic law of the radicals recombination $H+H+M \rightarrow H_2+M$, the model with both quadratic and linear reaction pathways for H recombination, and the model which takes into consideration the hydroperoxyl radical. The paper is organized as follows. In section 2 the mathematical formulation is presented. In sections 3 and 4 the results of numerical analysis for the flame speed, structure and stability are described and discussed. The conclusions are presented in section 5.

2. Formulation and methods

We consider a thermal-diffusive adiabatic model for rich hydrogen-air flame in single spatial dimension that includes two steps: chain branching $3H_2+O_2 \rightarrow 2H_2O+2H$ and recombination $H+H+M \rightarrow H_2+M$. According to [3, 16] when the burning temperature is not too high the concentrations of O, OH, and H_2O_2 are small, the elementary reaction related to them can be

neglected and the rates of the gross reactions are controlled by the following three elementary steps

$$\begin{aligned} \omega_I &= w_1 + \alpha w_4, \\ \omega_{II} &= w_4 + w_5. \end{aligned} \tag{1}$$

The rates w_1 ($H + O_2 \rightarrow OH + O$), w_4 ($H + O_2 + M \rightarrow HO_2 + M$), and w_5 ($H+H+M \rightarrow H_2+M$) are taken from either San-Diego kinetic mechanism [7] (results will be labelled with 'SD') or from [8] (results will be labelled with 'WB'). The reaction constants can be written as $k_i(T) = A_i e^{E_i/RT}$, where $A_i(T) = A_i(T_0)(T/T_0)^{n_i}$ are the pre-exponential factors and $T_0 = 298K$. The expression for α is derived in [16, 3] using the steady-state equations for O, OH, and HO_2 as $\alpha = (k_7 + k_8)(k_6 + k_7 + k_8 + k_9[OH]/[H])^{-1}$. Reactions $6-9$ which involve HO_2 are numerated as in [4]. The rate constants required to estimate α are taken from [31].

According to [3], the dimensional equations governing this process can be written as

$$\begin{aligned} \rho c_p \frac{\partial T}{\partial t} &= \lambda \Delta T + q_I \omega_I + q_{II} \omega_{II}, \\ \rho \frac{\partial Y_{O_2}}{\partial t} &= \rho D_{O_2} \Delta Y_{O_2} - W_{O_2} \omega_I, \\ \rho \frac{\partial Y_H}{\partial t} &= \rho D_H \Delta Y_H + 2 W_H (\omega_I - \omega_{II}), \end{aligned} \tag{2}$$

where $\Delta = \partial^2/\partial x^2$; T is the temperature; Y_{O_2} and Y_H represent the mass fraction of O_2 and H respectively; ρ is the density; λ is the thermal conductivity; c_p is the specific heat; D_{O_2} and D_H represent the diffusivities of the molecular oxygen and hydrogen radicals respectively; W_H and W_{O_2} represent the molecular weights of H and O_2; q_I is the specific heat of the branching whereas q_{II} represents the specific heat of the recombination reaction; E is the activation energy for the chain branching reaction; R is the universal gas constant. Eqs. (2) are considered subject to boundary conditions

$$\begin{aligned} &T = T_a, \qquad Y_{O_2} = Y_{O_2}^{\infty}, \qquad Y_H = 0 \quad \text{for} \quad x \rightarrow +\infty, \\ &\partial T/\partial x = 0, \quad \partial Y_{O_2}/\partial x = 0, \quad Y_H = 0 \quad \text{for} \quad x \rightarrow -\infty, \end{aligned} \tag{3}$$

which correspond to a wave travelling in the positive x-axis direction. Upstream, on the right boundary, T is equal to the ambient temperature, T_a;

oxygen has not been consumed yet and Y_{O_2} is equal to its maximal initial value in the cold unreacted mixture, $Y_{O_2}^{\infty}$; no radicals have been produced i.e. $Y_H = 0$. Downstream, on the left boundary, we require that there is no reaction happening, so the solution reaches a stationary point of Eq. (2). Therefore the zero flux conditions for T, Y_{O_2}, and zero condition for Y_H are imposed.

Introducing the nondimensional time, $t' = (\rho A_1/e^{\beta}\beta M^*)t$, coordinate $x' = (\rho^2 A_1 c_p/\lambda M^* \beta e^{\beta})^{1/2} x$, variables

$$\theta = \frac{T}{T^*\beta}, \quad y_{O_2} = \frac{Y_{O_2}}{Y_{O_2}^{\infty}}, \quad y_H = \frac{W_{O_2} Y_H}{2 W_H Y_{O_2}^{\infty}}, \tag{4}$$

and dimensionless parameters

$$\beta = \frac{E c_p}{R q_{II} Y_{O_2}^{\infty}}, \quad L_{O_2,H} = \frac{\lambda}{D_{O_2,H}\rho c_p}, \quad R_i = \frac{2^{i-4} A_i [M] e^{1/\theta_b}}{A_1}, \tag{5}$$

where $i = 4, 5$; θ_b is the downstream temperature of the burned mixture; $[M]$ is the third body concentration, $M^* = W_{O_2}/Y_{O_2}^{\infty}$ and $T^* = q_{II} Y_{O_2}^{\infty}/W_{O_2} c_p$ is the reference mass and temperature respectively, β is the dimensionless activation energy, L_{O_2} and L_H are the Lewis numbers for O_2 and H-radicals respectively, we write Eqs. (2) and (3) omitting primes as

$$\begin{aligned} \theta_t &= \theta_{xx} + \Omega_2 + \frac{q_I}{q_{II}}\Omega_1, \\ y_{O_2 t} &= L_{O_2}^{-1} y_{O_2 xx} - \beta\Omega_1, \\ y_{Ht} &= L_H^{-1} y_{Hxx} + \beta\Omega_1 - \beta\Omega_2, \end{aligned} \tag{6}$$

and

$$\begin{aligned} &\theta = \theta_a, \quad y_{O_2} = 1, \qquad y_H = 0 \quad \text{for} \quad x \to +\infty, \\ &\theta = \theta_b, \quad \partial y_{O_2}/\partial x = 0, \quad y_H = 0 \quad \text{for} \quad x \to -\infty. \end{aligned} \tag{7}$$

The nondimensional reaction rates are

$$\begin{aligned} \Omega_1 &= y_{O_2} y_H e^{\beta - 1/\theta} + \alpha y_{O_2} y_H R_4 e^{\beta - 1/\theta_b}, \\ \Omega_2 &= R_4 y_{O_2} y_H w e^{\beta - 1/\theta_b} + R_5 y_H^2 e^{\beta - 1/\theta_b}. \end{aligned} \tag{8}$$

The physical values, ρ, D_i, c_p and λ, characterizing the gas mixture as well as reaction coefficients R_i are treated as constants and are evaluated at the

temperature equal to $1/2T_b$ [14] and pressure of $1atm$. For given mixture composition, ϕ, the burning temperature is calculated. Then the thermodynamic data for the elements of the gas mixture is obtained from the NIST database [32] at the temperature equal to the half of the burning temperature. This data is then used to calculate the physical properties of the mixture according to methods described in [33]. The quantities obtained using this approach, ρ, c_p and λ, correspond to specific mixture composition, while D_i represent diffusion coefficients of H or O_2 in the multicomponent mixture. The Lewis numbers $L_{O_2,H}$ are then calculated according Eq. 5 as functions of ϕ and are found to agree with the data reported in [3, 18] for the range of equivalence ratios considered in this work. In figure 1 the results of calculations of $L_{O_2,H}$ are presented, where the Lewis numbers are plotted as functions of equivalence ratio for all models considered in this work. The data for different models lie almost on top of each other. Parameter α only weakly depends on the mixture composition and changes from 0.837 to 0.846 for $\phi = 5$ and 9 respectively. The ratio of $q_I/q_{II} \approx 0.11$ and is a constant regardless of ϕ. The activation energy is almost a linear function of ϕ as it is shown in figure 1, where β is plotted for all four models and the data for the different models is, once again, found to be very close. The reaction constants, $R_{4,5}$, which appear in Eqs. (8), are calculated according to definition (5) with the kinetic data taken from [7] and [8]. The dependence of $R_{4,5}$ on the inverse of the burned temperature, θ_b, is presented in figure 2. The reaction rates are plotted in the logarithmic scale. It is seen that the functions $R_i(\theta^{-1})$ is almost linear, which agrees with Eqs. (5). The slight deviation from the linear behaviuor is caused by the dependence of the mixture density and A_i on θ_b. The governing equations (6) can be represented in the same form for all four models considered here. The difference between the models is illustrated in table 1 and is discussed in the next section.

In order to find the speed and the structure of combustion wave the problem (6)-(7) is reduced to a system of ordinary differential equations. The solution to the problem (6)-(7) is sought in the form of a traveling wave $\theta(x,t) = \theta(\xi)$, $y_{O_2}(x,t) = y_{O_2}(\xi)$, and $y_H(x,t) = y_H(\xi)$, where a coordinate in the moving frame, $\xi = x - ct$, is introduced and c is the speed of the travelling wave. Substituting the solution of this form into the governing

equations we obtain

$$\begin{array}{l} \theta_{\xi\xi} + c\theta_\xi + \Omega_2 + q_I/q_{II}\Omega_1 = 0, \\ L_{O_2}^{-1} y_{O_2\xi\xi} + c y_{O_2\xi} - \beta\Omega_1 = 0, \\ L_H^{-1} y_{H\xi\xi} + c y_{H\xi} + \beta\Omega_1 - \beta\Omega_2 = 0. \end{array} \tag{9}$$

Now, we multiply the first equation by β, add it to the second equation for y_{O_2} multiplied by $1+q_I/q_{II}$ and the third equation for y_H in Eqs. (9) and integrate it once with respect to ξ over $(-\infty, +\infty)$. This yields a condition: $\lim_{\xi\to-\infty} S = \lim_{\xi\to+\infty} S$, where $S = \beta\theta + (1 + q_I/q_{II})y_{O_2} + y_H$. Combining this condition with Eqs. (7) results in the following expression for burned temperature $\theta_b = \theta_a + (1 + q_I/q_{II})/\beta$. The system of ordinary differential equations together with Eqs. (7) constitute the two-point boundary value problem, which is solved numerically by using a standard shooting algorithm with a fourth order Runge-Kutta integration scheme first and then the results are corrected by employing the relaxation algorithm.

The stability of the combustion waves is investigated in a way similar to [26]. We linearize the governing Eqs. (6) near the travelling wave solution. We seek solution of the form $\theta(x,t) = U(\xi) + \epsilon\phi(\xi)e^{\lambda t}$, $y_{O_2}(x,t) = V(\xi) + \epsilon\psi(\xi)e^{\lambda t}$, and $y_H(x,t) = W(\xi) + \epsilon\chi(\xi)e^{\lambda t}$, where $[U(\xi), V(\xi), W(\xi)]$ represent the travelling combustion wave. Here terms proportional to the small parameter ϵ are the linear perturbation terms, λ is a spectral parameter governing the time evolution of the perturbation. Substituting this expansion into Eq. (6), leaving terms proportional to the first order of ϵ only, and introducing the vector function with components $\mathbf{v}(\xi) = [\phi,\ \psi,\ \chi,\ \phi_\xi,\ \psi_\xi,\ \chi_\xi]^T$ we obtain

$$\mathbf{v}_\xi = \hat{A}(\xi, \lambda)\mathbf{v}, \tag{10}$$

where

$$\hat{A} = \begin{bmatrix} 0 & \hat{I} \\ \hat{H} + \lambda\hat{Q} & -c\hat{Q} \end{bmatrix}, \quad \hat{Q} = \begin{bmatrix} 1 & 0 & 0 \\ 0 & L_{O_2} & 0 \\ 0 & 0 & L_H \end{bmatrix}, \tag{11}$$

Here $H(\xi)$ is a Wronskian of source terms in Eqs. (6) calculated at $U(\xi)$, $V(\xi)$, $W(\xi)$ and $\hat{I}$ is 3×3 identity matrix. We will call a set, Σ, of all λ values for which there exists a solution to Eq. (10) bounded for both $\xi \to \pm\infty$ a spectrum of linear perturbations. In the general case, Σ is a set on the complex plane and it consists of the essential and the discrete spectrum. If there exists at least one $\lambda \in \Sigma$ such that $\mathrm{Re}\lambda > 0$, then the travelling wave solution is linearly unstable, otherwise, if for all $\lambda \in \Sigma$ the

real parts are not positive, then the travelling wave solution is linearly stable. Therefore in order to investigate the linear stability of the travelling wave solutions to Eq. (6), the spectrum Σ of the problem (10) has to be found. It can be shown (see [34] for details) that the essential spectrum consists of parabolic curves in the complex plane with $\mathrm{Re}\lambda \leq 0$. This implies that it is the discrete spectrum of the problem (10) that is responsible for the emergence of instabilities. The linear stability problem is solved by finding the location of the discrete spectrum on the complex plane using the Evans function method [34].

The nonlinear stability analysis as well as the properties of the solutions bifurcating from the travelling waves are investigated by direct integration of Eqs. (6). For our numerical algorithm we use the method of splitting with respect to the physical processes. Initially we solve the set of ordinary differential equations which describe the temperature and the species concentration variations due to the branching and recombination reactions by using the fourth order Runge-Kutta algorithm. As a next step, equations of heat and mass transfer for fuel and radicals are solved with the Crank-Nicholson method of the second-order approximation in space and time. The initial conditions for the numerical scheme are taken in a form of the traveling wave solution (or autowave) of Eqs. (9).

3. Travelling waves

In this section the results of numerical analysis for the three models discussed earlier are presented.

3.1. ZL model

Firstly, we consider the model proposed in [9, 10] which includes two overall steps with the rates, $\omega_{I,II}$ controlled by the elementary reactions w_1 $(H + O_2 \rightarrow OH + O)$ and w_5 $(H + H + M \rightarrow H_2 + M)$ respectively i.e. $\omega_I = w_1$ and $\omega_{II} = w_5$. It is assumed that H is the only radical involved in the reaction, and the concentrations of all other intermediates are insignificant. The first reaction is considered to possess a large activation energy and negligible heat of the reaction whereas, the recombination reaction has zero activation energy and is exothermic. Taking this into account R_5, α, q_I are considered to vanish in Eqs. (6). It is shown in [26] that the model can be written in the form of the Zeldovich-Liñán model therefore it will be referred to as the ZL-model.

In figure 3 the dependence of the flame speed, c, on the equivalence ratio of the mixture, ϕ, is plotted. Here and thereafter in this paper normal conditions for the ambient temperature, T_a, and pressure, P, are implied i.e. $T_a = 298K$ and $P = 1atm$. The speed is shown in dimensional units - meters per second. The solid lines represent the numerical results obtained here. The curves marked with the index 'SD' or 'WB' correspond to the choice of reaction constants as in [7] or in [8] respectively. As is seen the calculations with the reference data from [8] gives systematically smaller flame speed as compared to the calculations based on the data from [7]. The reaction rate, R_5, utilizing the 'SD'-scheme is less than the corresponding reaction rate using the 'WB'-scheme in the range of ϕ values considered here. As reported in [26] the increase of the rate of recombination reaction, R_5, shifts the combustion conditions towards the faster recombination regime, which results in the reduction of the flame speed. The symbols in figure 3 correspond to various experimental and numerical data from the literature [2, 15, 22, 35, 36, 37, 38] as referred in figure inlet. The ZL-model utilizing the 'SD' kinetic data gives a very good approximation for the flame speed.

The solution profiles for the mole fractions of oxygen, X_{O_2}, H radicals, X_H, and temperature, T, are plotted in figure 4 as functions of the coordinate, x, in the reference frame travelling with the combustion wave. The results are presented for $\phi = 5.57$, which corresponds to the hydrogen content of 70% in fresh mixture as in [19]. The mole fraction of H is multiplied by 4 in the figure so as to accommodate both X_{O_2} and X_H on the same graph. It is seen that the discrepancy between the 'SD' and 'WB' profiles of the H mole fractions is significant. The maximal values of H content are $\max X_H^{SD} \approx 0.0079$ and $\max X_H^{WB} \approx 0.0039$, whereas the detailed kinetics calculations [19] give $\max X_H^{Det} \approx 0.0078$. Once again we see that the results obtained with the ZL-model based on the 'SD' kinetic data provides an accurate approximation of the flame structure. The significant reduction of X_H for the model with 'WB' kinetics can also be explained by the larger value of the recombination reaction rate in comparison to the corresponding term using the 'SD' data. The faster consumption of H radicals in this case causes the decrease of the X_H.

The stability of the combustion wave has been investigated by using the Evans function method as outlined in section 2. We have found the flame to be stable with respect to pulsating (longitudinal) perturbations for the whole range of equivalence ratios considered here. This is not surprising since in [26] it was shown that the neutral stability boundary for combustion waves

in the Zeldovich-Liñán model shifts to large values of activation energy as the Lewis number for fuel is decreased. The limiting component is O_2 in our case and the corresponding Lewis number, L_{O_2}, is about 2. High activation energy correspond to large ϕ for the model considered here. Thus the neutral stability boundary moves to ϕ values much greater then $\phi = 7 - 8$ reported in the literature [2, 15, 20, 21, 22].

3.2. ZLD model

As a next step, the ZL-model considered above is modified to include the linear recombination step with respect to the H concentration. Such an extension is discussed in [39]. In this case the two gross steps with the rates, $\omega_{I,II}$, are controlled by elementary reactions w_1 ($H + O_2 \rightarrow OH + O$), w_4 ($H + O_2 + M \rightarrow HO_2 + M$), and w_5 ($H + H + M \rightarrow H_2 + M$) i.e. $\omega_I = w_1$ and $\omega_{II} = w_4 + w_5$. As in the previous case it is assumed that H is the only radical involved in the reaction. The first reaction is considered to have a large activation energy and negligible heat of the reaction whereas, the recombination reaction has zero activation energy and is exothermic. Formally this implies that in Eqs. (6), parameters α and, q_I are equal to zero. The model will be referred to as the ZLD-model.

The governing equations for the ZLD-model are solved numerically. The results of the analysis are presented in figure 5 where the dependence of the flame speed, c, on the equivalence ratio of the mixture, ϕ, is plotted. Once again the symbols in figure 5 correspond to data from the literature [2, 15, 22, 35, 36, 37, 38] as referred in figure inlet. The solid curves represent the results of the current work. The curves marked with the index 'SD' or 'WB' correspond to the choice of reaction constants as in [7] or in [8] respectively. The inclusion of the reaction $H + O_2 + M \rightarrow HO_2 + M$ intensifies the recombination of H radicals substantially. As a result the qualitative behaviour of the dependence of the flame speed for this model on the equivalence ratio changes. As ϕ approaches a certain finite value the flame speed vanishes and the combustion wave extinguishes. This is shown in figure 5, where both the 'SD' and 'WB' curves cross the $c = 0$ axis. Similar behaviour is discussed in [3] and also reported in [29] for the Dold model, which also has a linear dependence of the rate of the recombination reaction on the concentration of radicals.

The rate of the reaction $H + O_2 + M \rightarrow HO_2 + M$ can be written in dimensionless form as $w_4 = R_4 y_{O_2} y_H e^{\beta - 1/\theta_b}$, whereas the rate of radicals production via the reaction $H + O_2 \rightarrow OH + O$ is $w_1 = y_{O_2} y_H e^{\beta - 1/u}$. Hence,

there is a crossover temperature, θ^*, at which the rates of w_1 and w_4 are equal. For moderate values of ϕ the process is sufficiently exothermic and $\theta_b > \theta^*$. However, as ϕ is increased and the combustion becomes less exothermic the burning temperature approaches the crossover temperature. As a result the flame must extinguish as the mixture gets richer. The onset of extinction is enhanced by the recombination reaction w_5. The numerical calculations show that the combustion wave exhibits extinction for the ZLD model at the values of ϕ around six for both choices of reaction constants.

The Evans function analysis shows that the inclusion of w_4 reaction promotes the onset of pulsating instability. Thus the role of the reaction 4 is twofold. It shifts both the extinction and neutral stability boundary towards smaller values of ϕ. We consider the pre-exponential constants of the reactions 4 and 5 as free parameters in order to develop a model which fits both the flame speed and stability as predicted by the calculation with detailed kinetics. For definiteness the results of [2] are taken as the target data of such an analysis and the 'SD' kinetic constants are used. The model will be referred to as the PN-model. The rates of the reactions have to be substantially reduced in order to fit the data of [2], which predict the onset of pulsations for ϕ between 7.3 and 7.4. The best fit was found for $A_4^{PN} = 0.0655 A_4^{SD}$ and $A_5^{PN} = 0.117 A_5^{SD}$. The dependence of the flame speed on ϕ for the PN -model is shown in figure 5 with the curve marked 'PN'. As expected it approaches the results of [2] plotted with the empty circles for equivalence ratios close to 7. The curve shows the stable solution and is discontinued once it becomes unstable for $\phi = 7.31...$ The Evans function method allows the prediction of the frequency of pulsations which emerge as a result of the Hopf bifurcation [5]. We have found $f \approx 64 Hz$ in our calculations, whereas in [2, 20] it is reported to be around $80 Hz$. The earlier papers [15, 21] predict much smaller frequencies of about $12 - 30 Hz$. It should be noted that the frequency of nonlinear oscillations can depend on the amplitude, particularly, when the amplitudes are large. However here and later on we only discuss the frequencies of small pulsations just beyond the critical parameter values for the Hopf bifurcation when the amplitude of pulsations is small. The solution profiles for the PN-model are plotted in figure 4 with solid lines. It should be noted that the PN-model overestimates the maximum value of H for $\phi = 5.57$, that is $\max X_H^{PN} \approx 0.014$.

3.3. CL model

The model that admits the role of hydroperoxyl radical was proposed by Liñán. It is formulated in [16], studied in [3] and will be referred to as the 'CL' model. From the point of view of kinetics it assumes that H is also consumed by the reactions involving HO_2. This is taken into account in Eqs. (1) by the term proportional to α in the expression for the rate of the global reaction ω_I. It is also considered that the heat of the branching reaction, q_I, is not negligible.

The flame speed is found by numerically solving the governing equations (9) subject to boundary conditions (7). The results are presented in figure 6, where the dependence of the flame speed, c, on the equivalence ratio of the mixture, ϕ, is plotted. The meaning of the symbols and notations is the same as in figures 1 and 4. The stability analysis is also carried out by using the Evans function method. The solid lines correspond to the stable solutions, whereas the dashed lines show the unstable solution branches. The location of the points at which the stability changes are marked with filled squares on the 'SD' and 'WB' curves. It is seen that the predictions of the flame speed calculated with both 'SD' and 'WB' kinetic schemes are located between the results of [15] and [2] for values of ϕ greater than 8. For smaller values of the equivalence ratio the 'CL' model tends to over predict the flame velocity as compared to the results reported in the literature cited in the figure. The onset of pulsations is found at $\phi = 7.32$ and $\phi = 7.82$ when 'SD' and 'WB' reaction constants are used respectively. These results correlate with the data from the calculations with detailed kinetics [2, 3, 4, 15, 20, 21, 22]. The Hopf frequency for the 'SD' reaction scheme is found to be $220Hz$, whereas for the 'WB' kinetic scheme it is $70Hz$. The substantially higher value of the frequency of oscillation corresponding to the 'SD' reaction constants is due to the fact that the nondimensional time is inversely proportional to reaction constant, A_1, which is almost 3 times higher for the 'SD' mechanism as compared to the 'WB' mechanism.

In figure 7 the solution profiles for T, X_{O_2}, and X_H are plotted for $\phi = 5.57$. The solid and the dashed lines correspond to the 'SD' and 'WB' reaction schemes respectively. The molar concentration of H is multiplied by 10 so as to plot it on the same graph with X_{O_2}. The structure of the solutions is very close for both reaction schemes and also is in good agreement with the results of [19]. It should be noted that the burned temperature is higher than in figure 4. This is caused by the additional heat release, q_I, from the

branching reaction step, which has to be taken into account for the accurate estimate of the flame temperature.

4. Stability analysis

In this section we select three models i.e. the Zeldovich-Liñán-Dold with fitted rate constants (PN), Clavin-Liñán model with two choices of the rate constants (CL-SD and CL-WB) and study the stability of the deflagration waves in greater detail for these cases. The selection is based on the above analysis which indicates that the highlighted models are capable of predicting the flame speed and stability for rich mixtures.

In figure 8 the typical solution of the eigenvalue problem (10) is illustrated for the Clavin-Liñán model. As the neutral stability boundary is approached by increasing the equivalence ratio two complex conjugate points of the discrete spectrum move from the left to the right half of the complex plane causing the loss of stability of the travelling wave solution due to occurrence of the Hopf bifurcation. We will denote the critical value of the equivalence ratio at which this bifurcation occurs as ϕ_h. In figure 8 the real and imaginary part of λ is plotted against the difference of ϕ from the critical value ϕ_h with the solid and dashed lines respectively. Here only a single point of the discrete spectrum with positive imaginary λ is shown. As the bifurcation parameter, $\phi - \phi_h$, is increased the real $Re\lambda$ grows resulting in the travelling wave solution becoming more unstable, whereas the $Im\lambda$, responsible for the frequency of oscillations decay.

In figure 9 the neutral stability boundary corresponding to the critical parameter values for the Hopf bifurcation is plotted in the initial temperature against the equivalence ratio parameter plane. The stable propagation of combustion waves is encountered for the parameter values located above the curves in each case. The temperature is measured in Kelvins. The stability results are obtained using the Evans function technique as discussed earlier. All curves show similar qualitative behaviour: the neutral stability boundary shifts to richer mixtures as the temperature is increased. The Clavin-Liñán model with kinetic data from [8] overestimates the region of stability, while the CL model with 'SD' reaction constants and the phenomenological ZLD model are in better agreement especially for the ambient temperatures close to normal conditions. In figure 9 the Hopf frequencies, f, are also given for each curve at the initial temperature of $T_0 = 150K$ and the equivalence ratio $\phi = 11$. The eigenvalues, λ, of the linear stability problem Eq. 10 are

used to calculate f as $Im\lambda/2\pi$, where λ is taken at the critical condition for the loss of stability i.e. $Re\lambda = 0$. For $T_0 = 150K$ the Hopf frequencies are $f_{PN} \approx 89Hz$, $f_{CL-SD} \approx 400Hz$, and $f_{CL-WB} \approx 120Hz$, whereas for $\phi = 11$ they are $f_{PN} \approx 38Hz$, $f_{CL-SD} \approx 136Hz$, and $f_{CL-WB} \approx 36Hz$. It is clearly seen that the preheating of the unburned mixture results in lower Hopf frequencies. Also the Clavin-Liñán model with kinetic data from [8] (CL-WB) gives substantially higher estimates of the Hopf frequency.

As the neutral stability boundary is crossed in the parameter space the deflagration wave travelling without changing its speed and shape loses stability due to the Hopf bifurcation. The numerical integration of the governing Eqs. 6 suggest that the pulsating combustion regime of flame propagation emerge as a result of the Hopf bifurcation. This scenario was observed for all three models. The typical behavior of pulsating combustion wave in the PN model is illustrated in figure 10 for $\phi = 7.478$ and normal ambient conditions. The value of ϕ is taken above the critical value of the equivalence ratio for the Hopf bifurcation, $\phi_h = 7.31...$ The initial profile taken in the form of the traveling combustion wave is unstable and exhibits pulsating instabilities. These instabilities distort the solutions of Eqs. 6 at the initial stages of the evolution of the profile. There are transient peaks in the temperature distribution in the coordinate space and oscillations of the shape and maximum value of the mass fraction of the H profile, $\max\{X_H\}$. The X_{O_2} profile is mainly affected in the variation of the front curvature although some small oscillations of the mass fraction of O_2 are also observed in the product region.

To study the pulsating behaviour further it is useful to introduce $\xi = x - c_{drift}t$, a coordinate in the frame traveling with speed c_{drift} which is the mean value of the flame propagation velocity $c_{drift} = \lim_{t\to\infty} x_{max}/t$, where x_{max} is the coordinate of the maximum of the H mass fraction in the laboratory coordinate frame. The value of $\max X_H$ and the location of the maximum of the radical concentration ξ_{max} are convenient parameters to describe the pulsating nature of the solution.

As the pulsating instabilities evolve, the value of $\max X_H$ oscillate with an amplitude which initially grows exponentially with time. The frequency of these oscillations is given by the imaginary part $Im\lambda$ and the rate of exponential growth is determined by the real part, $Re\lambda$, of the pair of points of the discrete spectrum, responsible for the onset of instability. At times of the order of $(Re\lambda)^{-1}$, the amplitudes of oscillations, $\max X_H$, reach saturation and stabilize at certain values. The behavior of $T(\xi, t)$ and $X_{H,O_2}(\xi, t)$ profiles become periodic in time and so the pulsating combustion wave is formed. In

figure 10 the temperature and the mass fraction of H-radical profiles of the pulsating combustion wave are plotted respectively for three moments of time $t_1 = 0$ (solid), $t_2 = 3.148 \times 10^{-3}$ s (dash-dotted), and $t_3 = 1.25918 \times 10^{-2}$s (dashed). Since the solution is periodic, time is measured from 0 to T , where $T \approx 0.0223$ s is the period of oscillations.

In figure 11 the dependence of maximal value of mass fraction of H on time is plotted for the periodic pulsating combustion wave with $\phi = 7.478$. As we move away from the Hopf locus in the parameter space, by increasing ϕ from the critical value, the oscillations become more relaxational i.e. the $\max X_H(t)$ contains higher harmonics in a Fourier series expansion. It is seen in figure 11, where the oscillations are not harmonic and is characterized by sharp peeks and flat deeps. The increase of ϕ is also accompanied by the growth of the period of pulsations. Thus for $\max X_H$ the period $T \approx 0.0223$ s, while immediately after crossing the Hopf locus the period is 0.015625... s as it is discussed in section 3.2.

Next we investigate how the amplitude of oscillations of the function $\max\{X_H\}(t)$ depends on the bifurcation parameter ϕ. In order to do this for a given fixed value of ϕ we plot the minimum and maximum values of this function for the pulsating periodic combustion waves against the equivalence ratio in figure 12. For steady travelling combustion waves there are no pulsations and $\max\{X_H\}(t)$ is constant with time. These solution branches are shown with the thick solid curves. For the oscillatory solutions the minimum and maximum values of the peak value of X_H in the coordinate space are plotted as two dots. As seen in figure 12 that, as ϕ is increased beyond the Hopf bifurcation point, the amplitude of pulsations grows continuously and has a root-type behaviour. This type of behaviour is common for the supercritical Hopf bifurcation. The amplitude of pulsations grows faster for the PN model with the increase of ϕ from the Hopf value in comparison to the CL model.

The flame speed is also affected by the onset of pulsations. In figure 13 the dependencies of both c and c_{drift} on ϕ are plotted for travelling and pulsating solutions respectively. The stable solution branches are shown with the solid lines and the dotted lines represent the unstable travelling wave solutions, which become unstable owing to Hopf bifurcation. Immediately after the Hopf bifurcation the pulsating solution branches out from the travelling wave solution. As seen in figure 13 the pulsating wave on average travels slower than the traveling wave and the difference $c - c_{drift}$ is growing with increasing ϕ from the Hopf value.

5. Conclusions

We have considered four two-step chain-branching adiabatic models for premixed flame propagation in rich hydrogen-air flames in order to investigate the thermal-diffusive pulsating instability near the rich flammability limit. It was assumed that the reaction proceed in two overall steps, H is the only radical involved in the reaction. The first reaction is considered to have a large activation energy and small heat of the reaction whereas, the recombination reaction has zero activation energy and is exothermic.

In the Zeldovich-Liñán model the overall branching and termination reactions are controlled by elementary steps $H+O_2 \rightarrow OH+O$ and $H+H+M \rightarrow H_2+M$, respectively. The numerical analysis has shown that the model with kinetic data from [7] accurately predicts normal flame speed for rich mixtures as compared to the data obtained with the detailed kinetics calculations. However the combustion wave solutions was found to be stable up to very large values of equivalence ratio (over ten). This is not feasible according to the calculations with detailed kinetics [2, 15, 21, 22]. Therefore it is clear that this model is suitable for the study of stationary flame propagation problems only.

In the Zeldovich-Liñán-Dold model the overall recombination reaction is controlled by two elementary steps: $H + O_2 + M \rightarrow HO_2 + M$ and $H+H+M \rightarrow H_2+M$. The inclusion of the reaction $H+O_2+M \rightarrow HO_2+M$ intensifies the recombination of H radicals substantially. As a result the flame extinguishes at finite values of equivalence ratio of the order of six, which makes this particular model inappropriate for the study of rich hydrogen-air flames. However, based on the Zeldovich-Liñán-Dold model, we formulate the phenomenological model, where the rate constants of the reactions $H+O_2+M \rightarrow HO_2+M$ and $H+H+M \rightarrow H_2+M$ are considered as fitting parameters. This results in an approach which gives an accurate prediction of the flame speed near the flammability limit, the critical equivalence ratio for the onset of pulsating instabilities and the frequency of oscillations. The structure of the combustion wave also agrees reasonably well with the calculations based on the detailed kinetics. Although the phenomenological model tends to overestimate the concentration of the H radicals.

The Clavin-Liñán model assumes that H is also engaged in the reactions involving HO_2, although hydroperoxyl radicals are considered to be in steady state. As a result the rate of the global branching reaction is modified. The heat of the branching reaction is not vanishing as well. The resulting model

with the kinetic data from [8] is shown to give accurate predictions for the flame speed and structure, as well as stability and frequency of pulsations for large equivalence ratios. However, the model overestimates the flame speed for moderately rich hydrogen-air flames.

The Clavin-Liñán model and the Zeldovich-Liñán-Dold model with fitted rates of the reactions are chosen for further stability analysis since they demonstrate the capabilities of predicting the flame speed, structure and stability. The neutral stability boundary was found as a function the ambient temperature. It was shown that increasing the initial temperature extends the region of stable combustion to richer mixture compositions. The dependence of the Hopf frequency on the initial temperature is also investigated. It is found that the frequency of pulsations decay with the preheating of the fresh mixture. Also the Clavin-Liñán model with the kinetic data from [7] overestimates the Hopf frequency in comparison with the other models.

The Hopf bifurcation which is responsible for the loss of stability of the travelling combustion waves is further investigated. It is demonstrated to be supercritical and the stable pulsating combustion waves emerge as the neutral stability boundary is crossed due to the Hopf bifurcation. These regimes are characterized by oscillations of the peak values of the temperature and the H-radical concentrations profiles. The pulsating waves are periodic functions of time in the coordinate frame co-moving with average speed of the flame propagation. It is found that the average flame speed decreases faster than the traveling wave speed as the equivalence ratio is increased from the critical parameter values for the Hopf bifurcation. Also as we move away from the neutral stability boundary the period of oscillations and the amplitude of oscillations of the peak values of the H-profiles grow.

To summarize, our investigation of the various reduced models shows that the Clavin-Liñán model is suitable for the analysis of the complex pulsating dynamics of the hydrogen flames near the rich flammability limit. We plan to further verify the model against different pressure conditions in our future investigations.

6. Acknowledgements

V.V. Gubernov, A.V. Kolobov and A.A. Polezhaev would like to acknowledge the financial support from the Russian Foundation for Basic Research grant 11-01-00392 and the Dynasty Foundation. H.S. Sidhu would like to acknowledge the support of the Australian Research Council Grant DP0878146.

References

[1] G. Joulin, P. Clavin, Combustion and Flame 35 (1979) 139 – 153.

[2] E. Christiansen, C. Sung, C. Law, Symposium (International) on Combustion 27 (1998) 555 – 562.

[3] L. He, P. Clavin, Combustion and Flame 93 (1993) 391–407.

[4] L. He, P. Clavin, Combustion and Flame 93 (1993) 408–420.

[5] V. Gubernov, A. Kolobov, A. Polezhaev, H. Sidhu, G. Mercer, Proc. R. Soc. Lond. A 466 (2010) 2747–2769.

[6] G. N. Mercer, R. O. Weber, H. S. Sidhu, Proc. R. Soc. Lond. A 454 (1998) 2015–2022.

[7] P. Saxena, F. A. Williams, Combustion and Flame 145 (2006) 316–323.

[8] M. O. Conaire, H. J. Curran, J. M. Simmie, W. J. Pitz, C. K. Westbrook, International Journal of Chemical Kinetics 36 (2004) 603–622.

[9] Y. B. Zeldovich, Kinetika i kataliz 2 (1961) 305–318.

[10] G. Dixon-Lewis, Proc. R. Soc. Lond. A 298 (1967) 495–513.

[11] F. Mauss, N. Peters, B. Rogg, F. A. Williams, in: N. Peters & B. Rogg (Ed.), Lecture Notes in Physics, Berlin Springer Verlag, 1993, volume 15 of *Lecture Notes in Physics, Berlin Springer Verlag*, pp. 29–43.

[12] K. Seshadri, N. Peters, F. A. Williams, Combustion and Flame 96 (1994) 407 – 427.

[13] D. Fernández-Galisteo, G. del Alamo, A. Sánchez, A. Liñán, in: Proc. of the Third European Combustion Meeting 2007, 6-19, pp. 1–5.

[14] O. Korobeinichev, T. Bolshova, Combustion, Explosion, and Shock Waves 45 (2009) 507–510. 10.1007/s10573-009-0061-1.

[15] K. Kailasanath, K. Ganguly, G. Patnaik, in: Prog. in Astronautics and Aeronautics, volume 151, AIAA, Washington DC, 1993, pp. 247–262.

[16] P. Clavin, Prog. Energy Combust. Sci. 11 (1985) 1–59.

[17] P. Boivin, C. Jiménez, A. L. Sánchez, F. A. Williams, Proceedings of the Combustion Institute 33 (2011) 517 – 523.

[18] E. Hu, Z. Huang, J. He, H. Miao, Int. J. Hydrogen Energy (2009) 8741–8755.

[19] A. Ern, V. Giovangigli, Combust. Sci. Tech. 149 (1999) 157–181.

[20] E. W. Christiansen, C. K. Law, C. J. Sung, Combustion and Flame 124 (2001) 35–49.

[21] G. Goyal, U. Maas, J. Warnatz, Combust. Sci. and Tech. 105 (1995) 183–193.

[22] N. R. Carter, M. A. Cherian, G. Dixon-Lewis, in: N. Peters, J. Warnatz (Eds.), Numerical methods in Laminar Flame Propagation: A GAMM Workshop, Vieweg, 1982, pp. 182–191.

[23] Y. B. Zeldovich, Zhurnal Fizicheskoi Khimii 22 (1948) 27–48.

[24] A. Liñán, A Theoretical Analysis of Premixed Flame Propagation with an Isothermal Chain Reaction, Technical Report 1, Instituto Nacional de Tecnica Aeroespacial Madrid (Spain), 1971.

[25] J. W. Dold, R. O. Weber, R. W. Thatcher, A. A. Shah, Combustion Theory and Modelling 7 (2003) 175–203.

[26] V. V. Gubernov, A. V. Kolobov, A. A. Polehaev, H. S. Sidhu, Combustion and Flame 159 (2012) 1185–1196.

[27] J. W. Dold, Combustion Theory and Modelling 11 (2007) 909–948.

[28] G. J. Sharpe, SIAM Journal on Applied Mathematics 70 (2009) 866–884.

[29] V. V. Gubernov, A. V. Kolobov, A. A. Polezhaev, H. S. Sidhu, G. N. Mercer, Combustion Theory and Modelling 15 (2011) 385–407.

[30] V. N. Kurdyumov, D. Fernández-Galisteo, Combustion and Flame (2012 in press).

[31] J. A. Manion, R. E. Huie, R. D. Levin, D. R. Burgess Jr., V. L. Orkin, W. Tsang, W. S. McGivern, J. W. Hudgens, V. D. Knyazev, D. B. Atkinson, E. Chai, A. M. Tereza, C.-Y. Lin, T. C. Allison, W. G. Mallard, F. Westley, J. T. Herron, R. F. Hampson, D. H. Frizzell, in: NIST Standard Reference Database 17, Version 7.0 (Web Version), Release 1.4.3, Data version 2008.12, National Institute of Standards and Technology, Gaithersburg, Maryland, 20899-8320. Web address: http://kinetics.nist.gov/ (retrieved August 15, 2011).

[32] E. W. Lemmon, M. O. McLinden, D. G. Friend, in: P. Linstrom, W. Mallard (Eds.), NIST Chemistry WebBook, NIST Standard Reference Database Number 69, National Institute of Standards and Technology, Gaithersburg MD, 20899, http://webbook.nist.gov (retrieved August 15, 2011).

[33] R. C. Reid, J. M. Prausnitz, T. K. Sherwood, The properties of gases and liquids, McGraw, New York, 1987.

[34] B. Sandstede, in: B. Fiedler (Ed.), Handbook of Dynamical Systems II, Elsevier, North-Holland, 2002, pp. 983–1055.

[35] D. R. Dowdy, D. B. Smith, S. C. Taylor, A. Williams, Symposium (International) on Combustion 23 (1991) 325 – 332.

[36] F. Takahashi, M. Mizomoto, S. Ikai, in: T. N. Veziroglu (Ed.), Nuclear energy/synthetic fuels, New York: McGraw-Hill, 1983, p. 447457.

[37] G. Koroll, R. Kumar, E. Bowles, Combustion and Flame 94 (1993) 330 – 340.

[38] K. Aung, M. Hassan, G. Faeth, Combustion and Flame 109 (1997) 1 – 24.

[39] D. Fernández-Galisteo, A. L. Sánchez, A. Liñán, F. A. Williams, Combustion and Flame 156 (2009) 985 – 996.

7. List of tables

Table 1. Parameters α, q_I, and $R_{4,5}$ for the different models. The abbreviation ZL, ZLD, and CL corresponde to the Zeldovich-Liñán, Zeldovich-Liñán-Dold, and Clavin-Liñán models respectively. The nonzero parameter values are indicted as '+' and the superscripts provide the references to the corresponding equations or papers used to calculate the values of these parameters.

8. List of captions

Fig. 1 Dependence of the Lewis numbers for O_2 and H (left axis) and activation energy, β, (right axis) on the equivalence ratio, ϕ.

Fig. 2 Dependence of the reaction constants $R_{4,5}$ on the inverse of the burning temperature, θ_b, for the choice of kinetic constants as in [7] or in [8].

Fig. 3 Dependence of the speed, c, of combustion wave on the equivalence ratio for the ZL model. The solid lines represent the numerical results obtained here, whereas the symbols show various experimental and numerical data from the literature. The curves marked with the index 'SD' or 'WB' correspond to the choice of reaction constants as in [7] or in [8] respectively.

Fig. 4 Solution profiles for X_{O_2}, X_H and T as functions of coordinate x for $\phi = 5.57$. The solid lines correspond to the fitted model 'PN' discussed in section 3.2. The dotted and the dashed lines represent the results for the ZL model with the 'SD' or 'WB' scheme kinetic parameters.

Fig. 5 Dependence of the speed, c, of the combustion wave on the equivalence ratio for the ZLD model. The solid lines represent the numerical results obtained here, whereas the symbols show various experimental and numerical data from the literature. The curves marked with the index 'SD' or 'WB' correspond to the choice of reaction constants as in [7] or in [8] respectively. The curve marked 'PN' represents the results for ZLD model with fitted reaction rates.

Fig. 6 Dependence of the speed, c, of the combustion wave on the equivalence ratio for the CL model. The solid lines represent the numerical results obtained here, whereas the symbols show various experimental and numerical data from the literature. The curves marked with the index 'SD' or 'WB' correspond to the choice of reaction constants as in [7] or in [8] respectively. The unstable solution branches are shown with the dashed lines.

Fig. 7 Solution profiles for X_{O_2}, X_H and T as functions of coordinate x for $\phi = 5.57$. The solid and the dashed lines represent the results for CL model with 'SD' or 'WB' kinetic parameters respectively.

Fig. 8 The real and imaginary parts of the points of the discrete spectrum, λ, as functions of $\phi - \phi_h$ shown with the solid and dashed lines respectively. The results correspond to CL model with 'SD' or 'WB' kinetic parameters.

Fig. 9 Neutral stability boundary for the travelling combustion waves as a function of the equivalence ratio. The solid curve represents the results for ZLD model with fitted reaction rates. The dashed and the dashes-dotted lines correspond to the Clavin-Liñán model with the choice of reaction constants as in [7] ('SD') or in [8] ('WB') respectively.

Fig. 10 Pulsating combustion wave solutions for $\phi = 7.478$. The temperature (left axis) and radical mass fraction (right axis) profiles, $T(\xi)$ and $X_H(\xi)$, are plotted as functions of coordinate in co-moving frame. The profiles are sampled at $t_1 = 0$, $t_2 = 3.148 \times 10^{-3}$ s, and $t_3 = 1.25918 \times 10^{-2}$s, which correspond to the solid, dash-dotted, and dashed lines respectively.

Fig. 11 Time history of pulsations of maximum value of X_H for $\phi = 7.478$.

Fig. 12 Temporal maximum and minimum of the peak value of the molar fraction of H in space, $\max X_H$, as function of ϕ. The thick solid lines and dots connected with the thin solid lines represent the travelling wave and pulsating solutions respectively.

Fig. 13 Dependence of the flame speed, c, on the equivalence ratio for the PN, CL-SD, and CL-WB models. The solid lines represent the numerical results obtained here, whereas the symbols show various experimental and numerical data from the literature. The unstable solution branches are shown with the dashed lines.

Table1

Model	a	q_1	R_4	R_5
ZL	0	0	0	+[1]
ZLD	0	0	+[1]	+[1]
PN	0	0	+[2]	+[2]
CL	+[3]	+[3]	+[1]	+[1]

[1)] Reference [7,8], Eq. 5

[2)] Fitted coefficients, Eq. 5

[3)] Reference [3,16]

ϕ

Figure 1

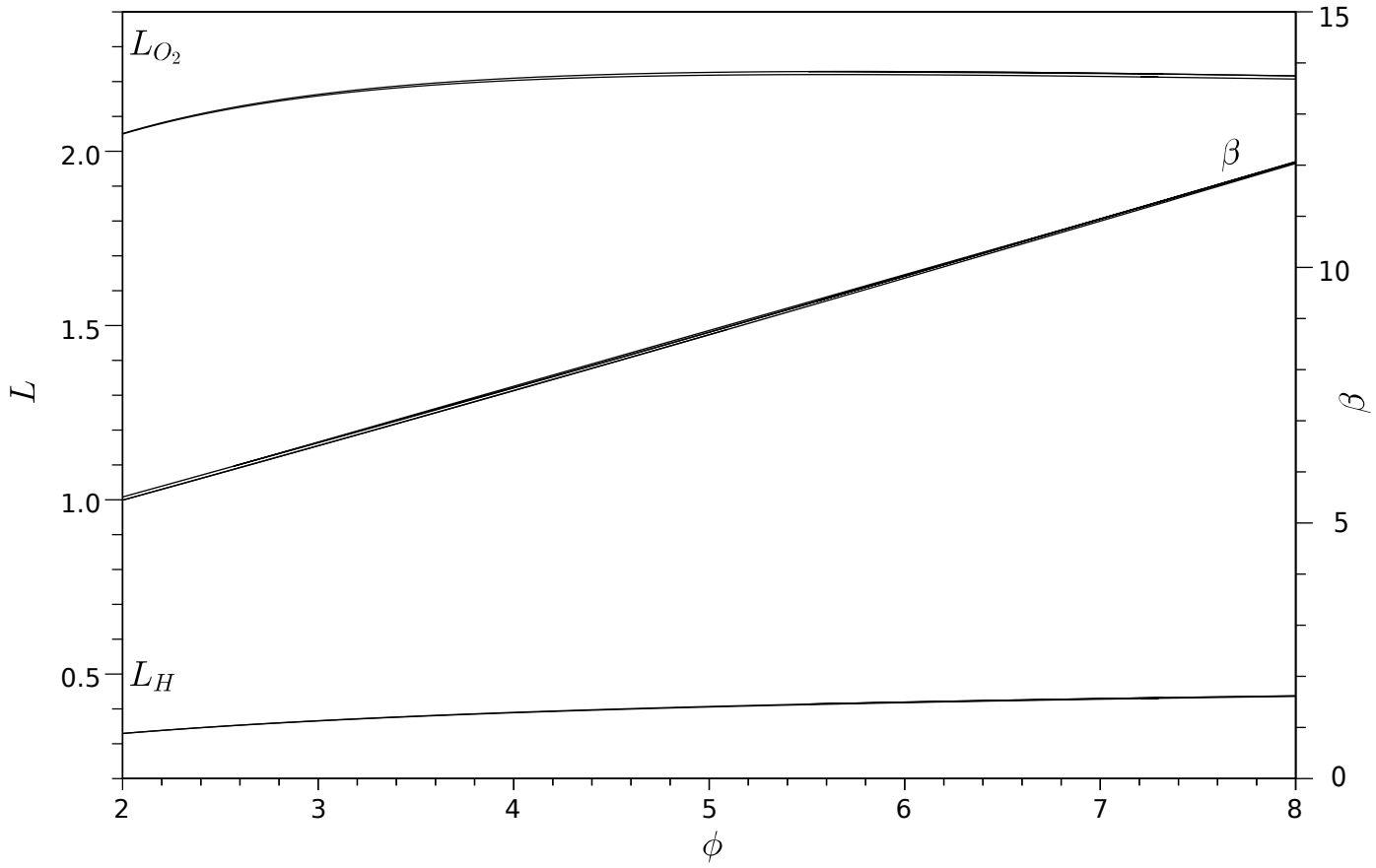

Figure 2

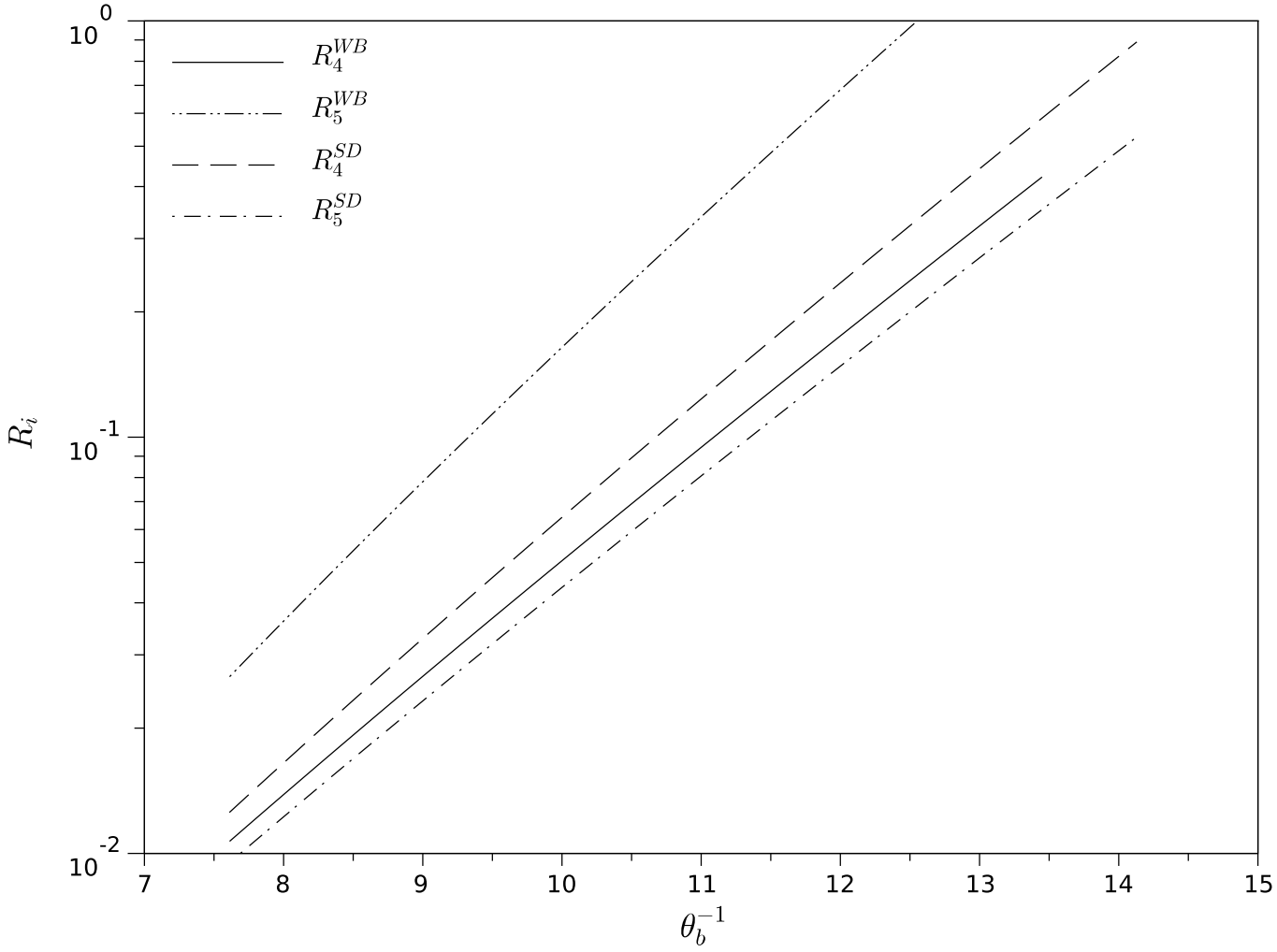

Figure 3

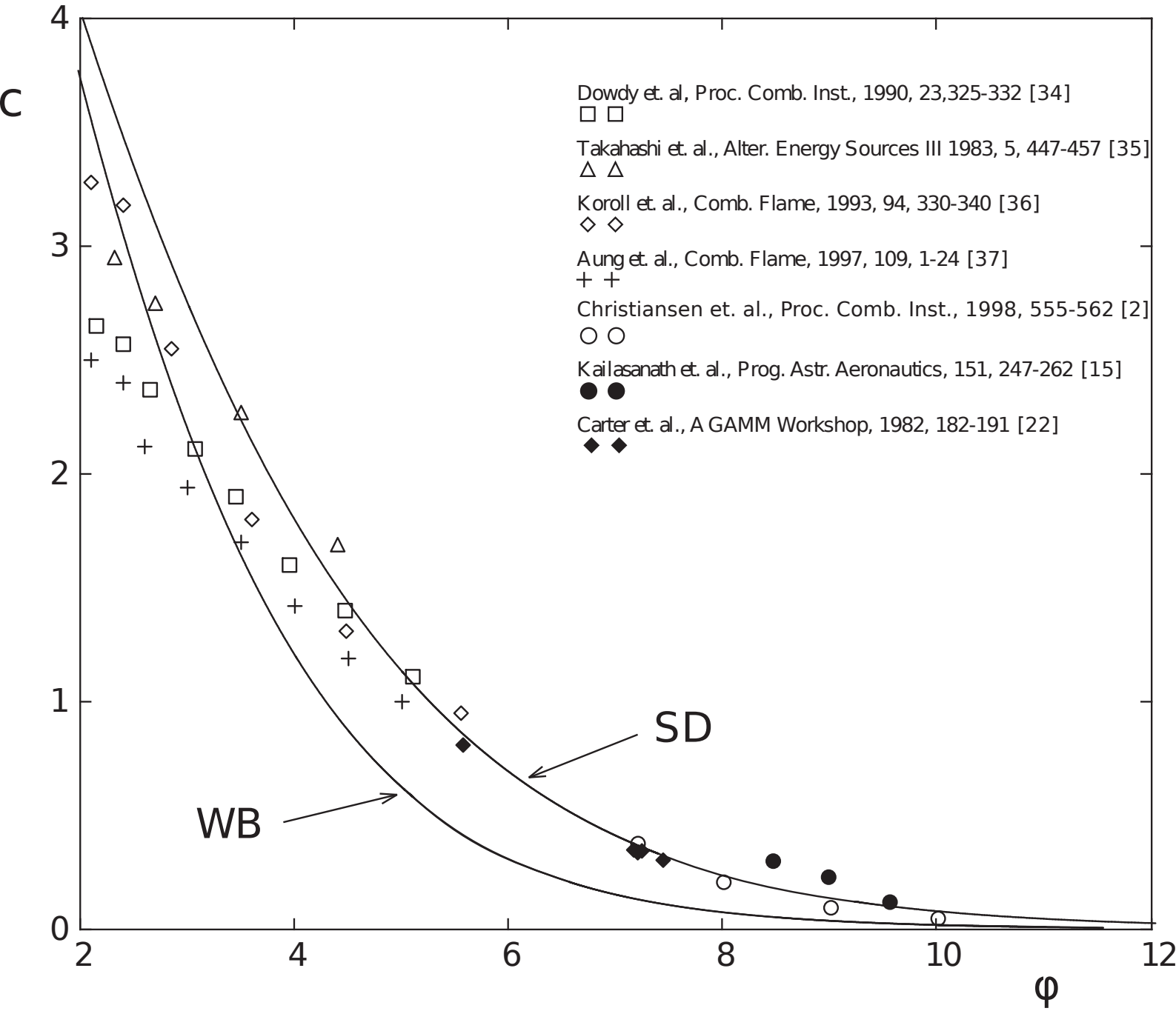
C
φ
SD
WB
Dowdy et. al, Proc. Comb. Inst., 1990, 23,325-332 [34]
Takahashi et. al., Alter. Energy Sources III 1983, 5, 447-457 [35]
Koroll et. al., Comb. Flame, 1993, 94, 330-340 [36]
Aung et. al., Comb. Flame, 1997, 109, 1-24 [37]
Christiansen et. al., Proc. Comb. Inst., 1998, 555-562 [2]
Kailasanath et. al., Prog. Astr. Aeronautics, 151, 247-262 [15]
Carter et. al., A GAMM Workshop, 1982, 182-191 [22]

Figure 4

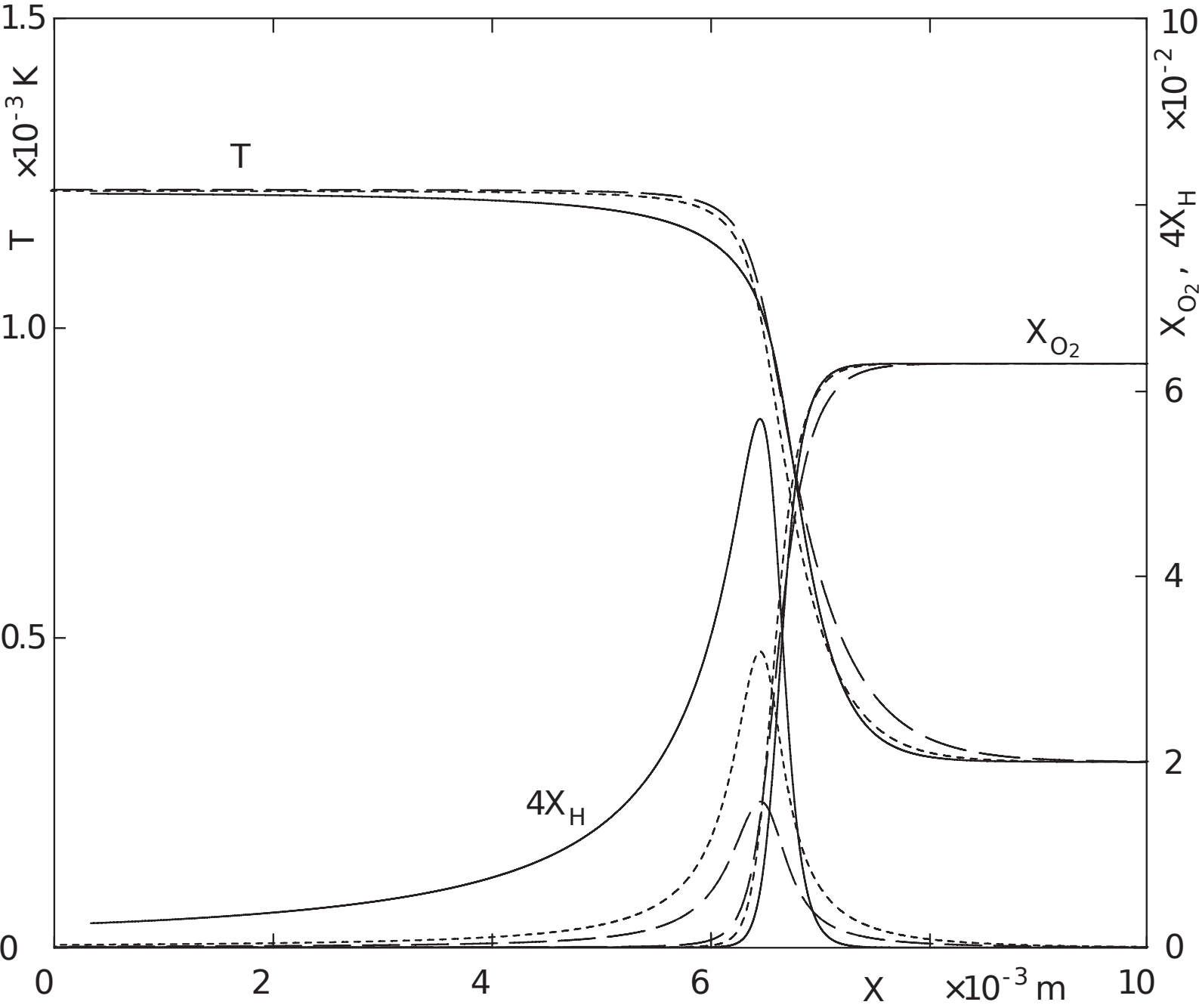

Figure 5

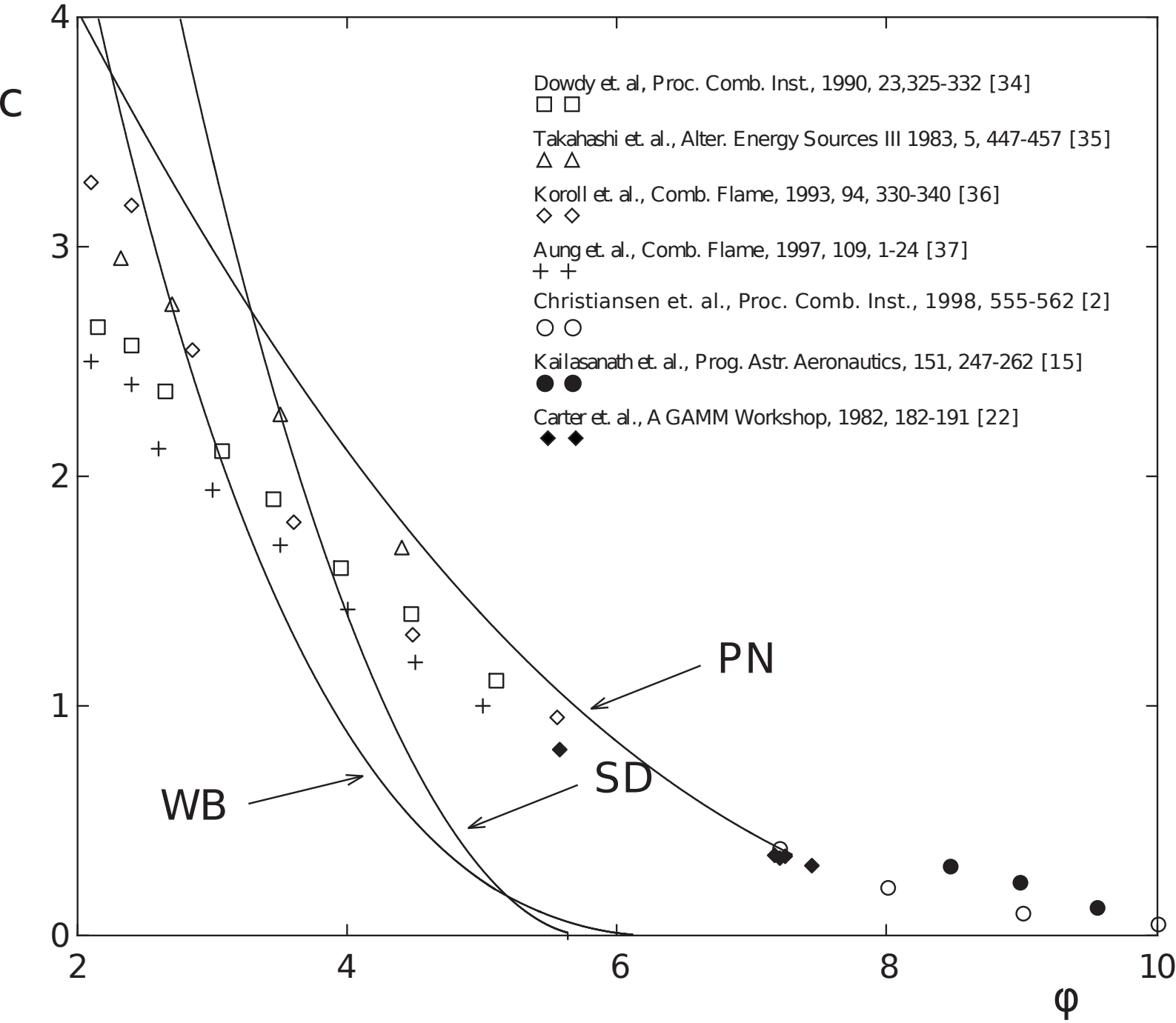
C
φ
0
1
2
3
4
2
4
6
8
10
Dowdy et. al, Proc. Comb. Inst., 1990, 23,325-332 [34]
Takahashi et. al., Alter. Energy Sources III 1983, 5, 447-457 [35]
Koroll et. al., Comb. Flame, 1993, 94, 330-340 [36]
Aung et. al., Comb. Flame, 1997, 109, 1-24 [37]
Christiansen et. al., Proc. Comb. Inst., 1998, 555-562 [2]
Kailasanath et. al., Prog. Astr. Aeronautics, 151, 247-262 [15]
Carter et. al., A GAMM Workshop, 1982, 182-191 [22]
PN
SD
WB

Figure 6

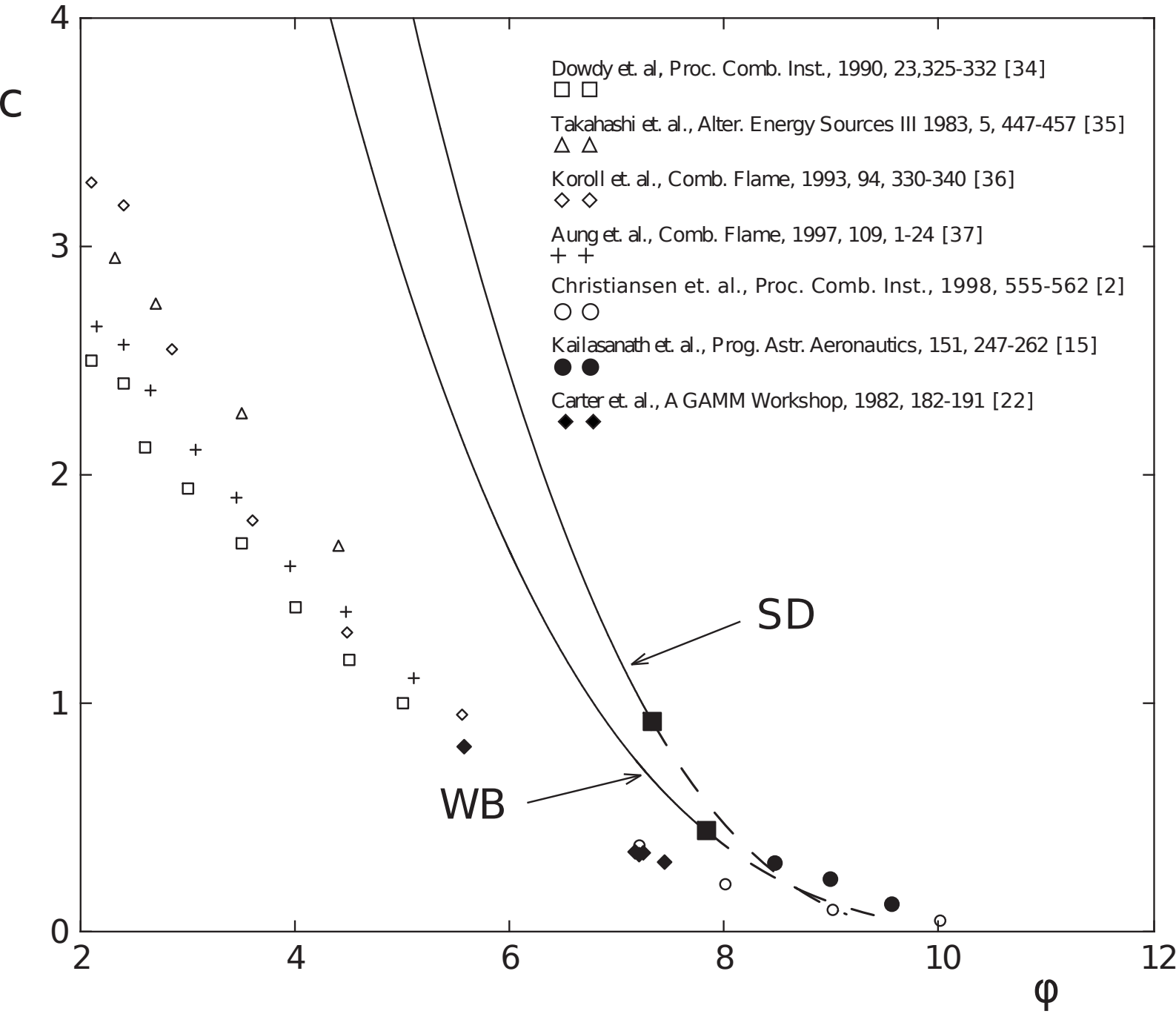
C
φ
SD
WB
Dowdy et. al, Proc. Comb. Inst., 1990, 23,325-332 [34]
Takahashi et. al., Alter. Energy Sources III 1983, 5, 447-457 [35]
Koroll et. al., Comb. Flame, 1993, 94, 330-340 [36]
Aung et. al., Comb. Flame, 1997, 109, 1-24 [37]
Christiansen et. al., Proc. Comb. Inst., 1998, 555-562 [2]
Kailasanath et. al., Prog. Astr. Aeronautics, 151, 247-262 [15]
Carter et. al., A GAMM Workshop, 1982, 182-191 [22]
0
1
2
3
4
2
4
6
8
10
12

Figure 7

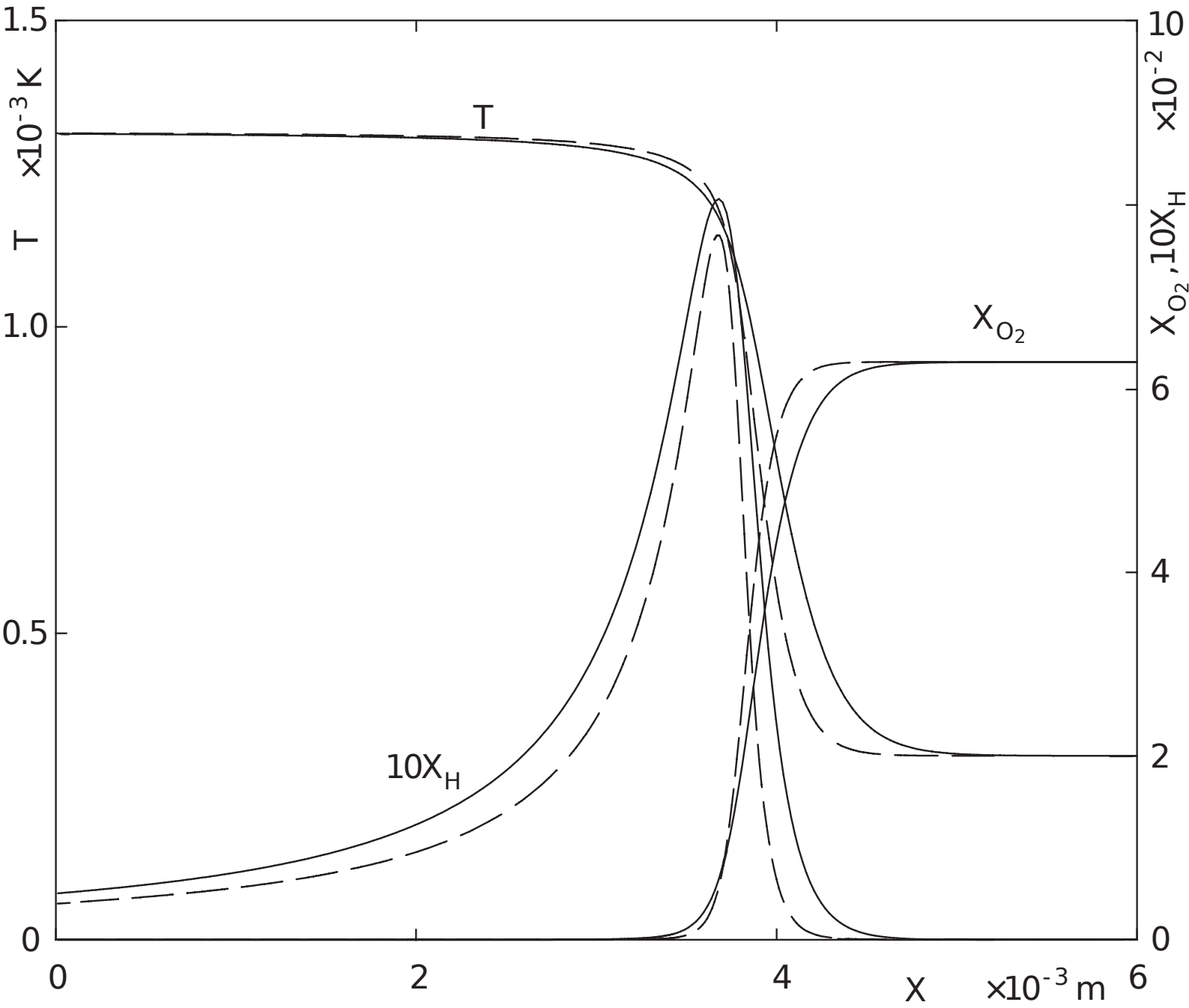

Figure 8

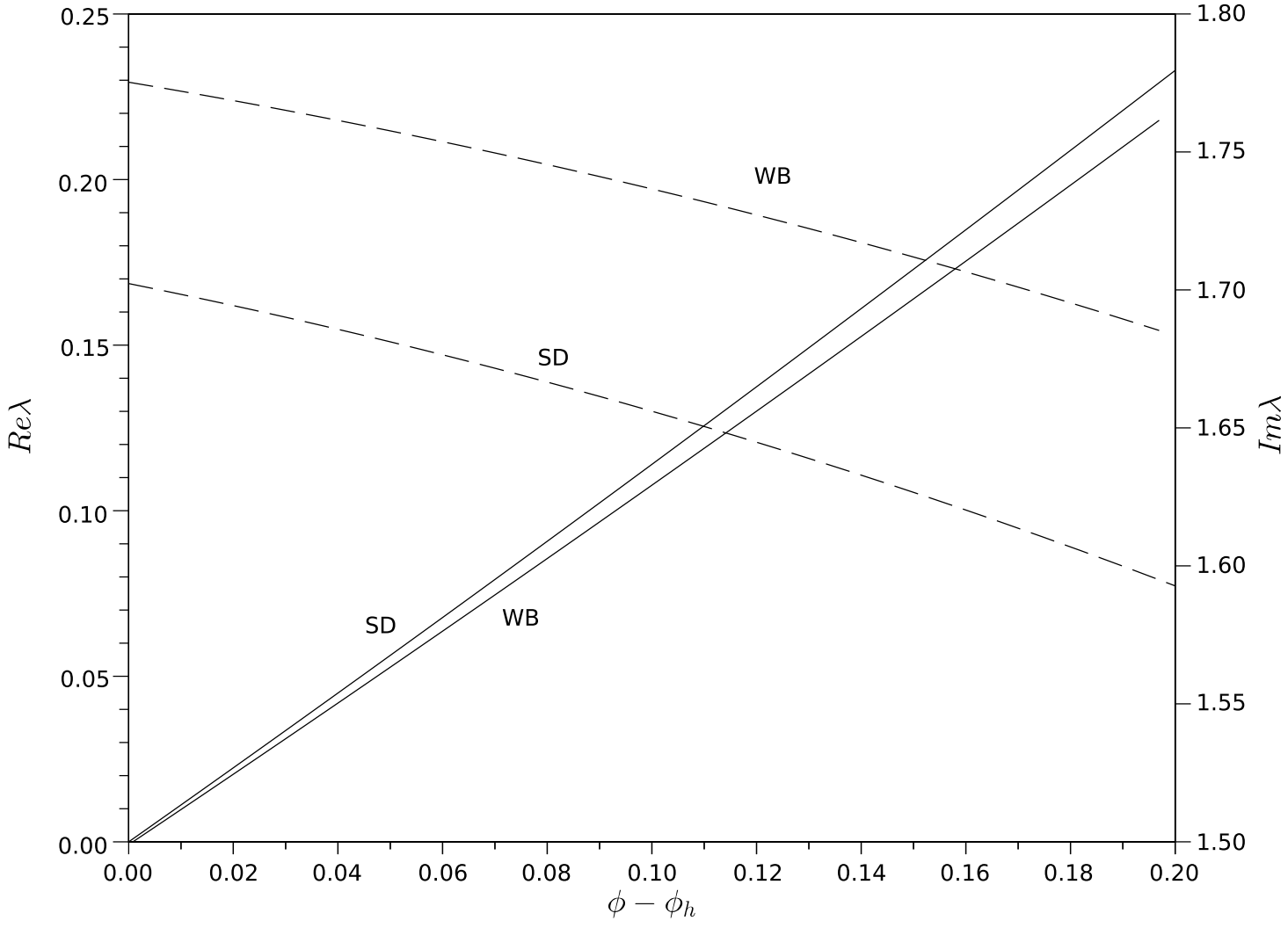
0.25
0.20
0.15
0.10
0.05
0.00
1.80
1.75
1.70
1.65
1.60
1.55
1.50
0.00
0.02
0.04
0.06
0.08
0.10
0.12
0.14
0.16
0.18
0.20
$Re\lambda$
$Im\lambda$
$\phi - \phi_h$
WB
SD
SD
WB

Figure 9

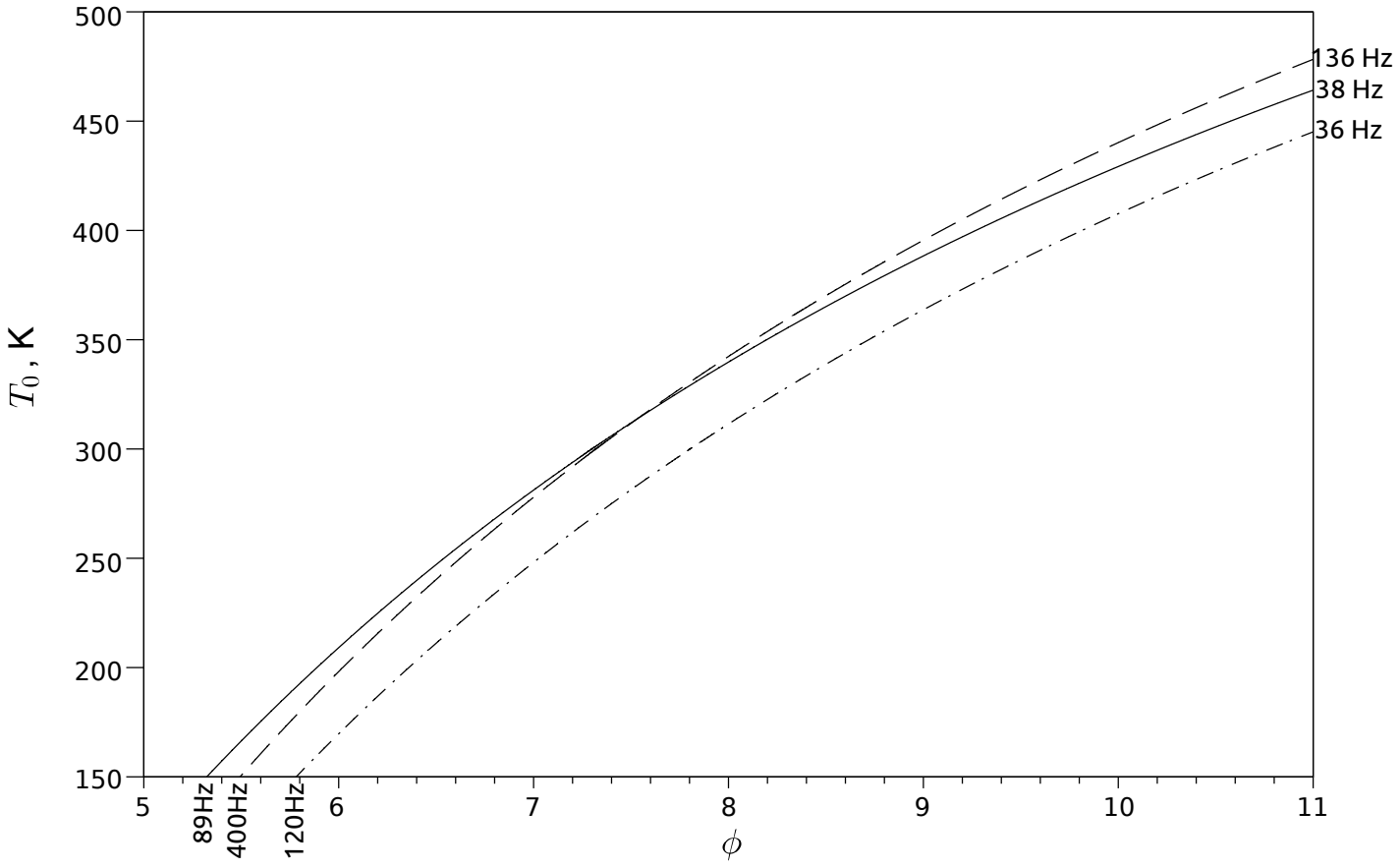
500
450
400
350
300
250
200
150
T_0, K
5
6
7
8
9
10
11
ϕ
89Hz
400Hz
120Hz
136 Hz
38 Hz
36 Hz

Figure 10

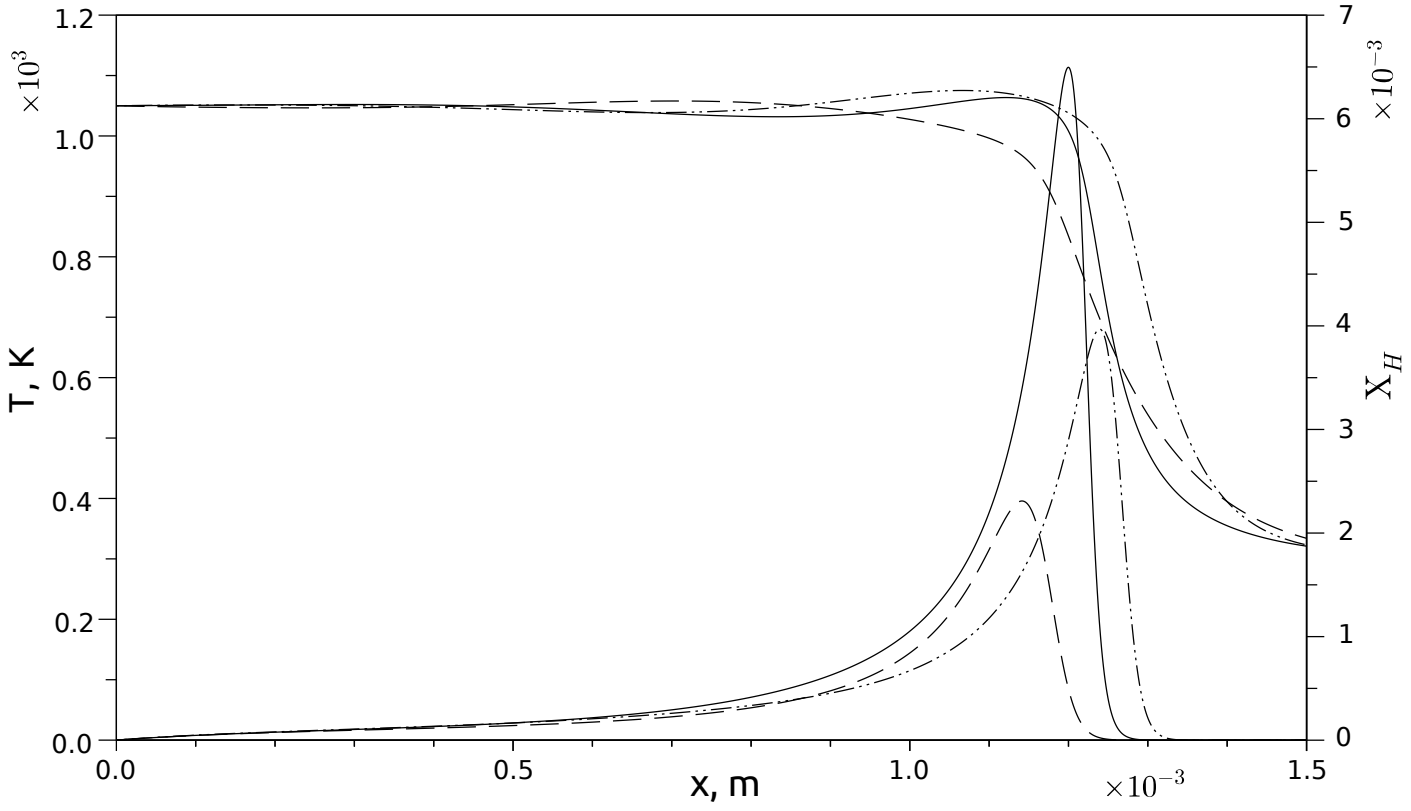
1.2
1.0
0.8
0.6
0.4
0.2
0.0
$\times 10^3$
T, K
0.0
0.5
1.0
1.5
x, m
$\times 10^{-3}$
7
6
5
4
3
2
1
0
$\times 10^{-3}$
X_H

Figure 11

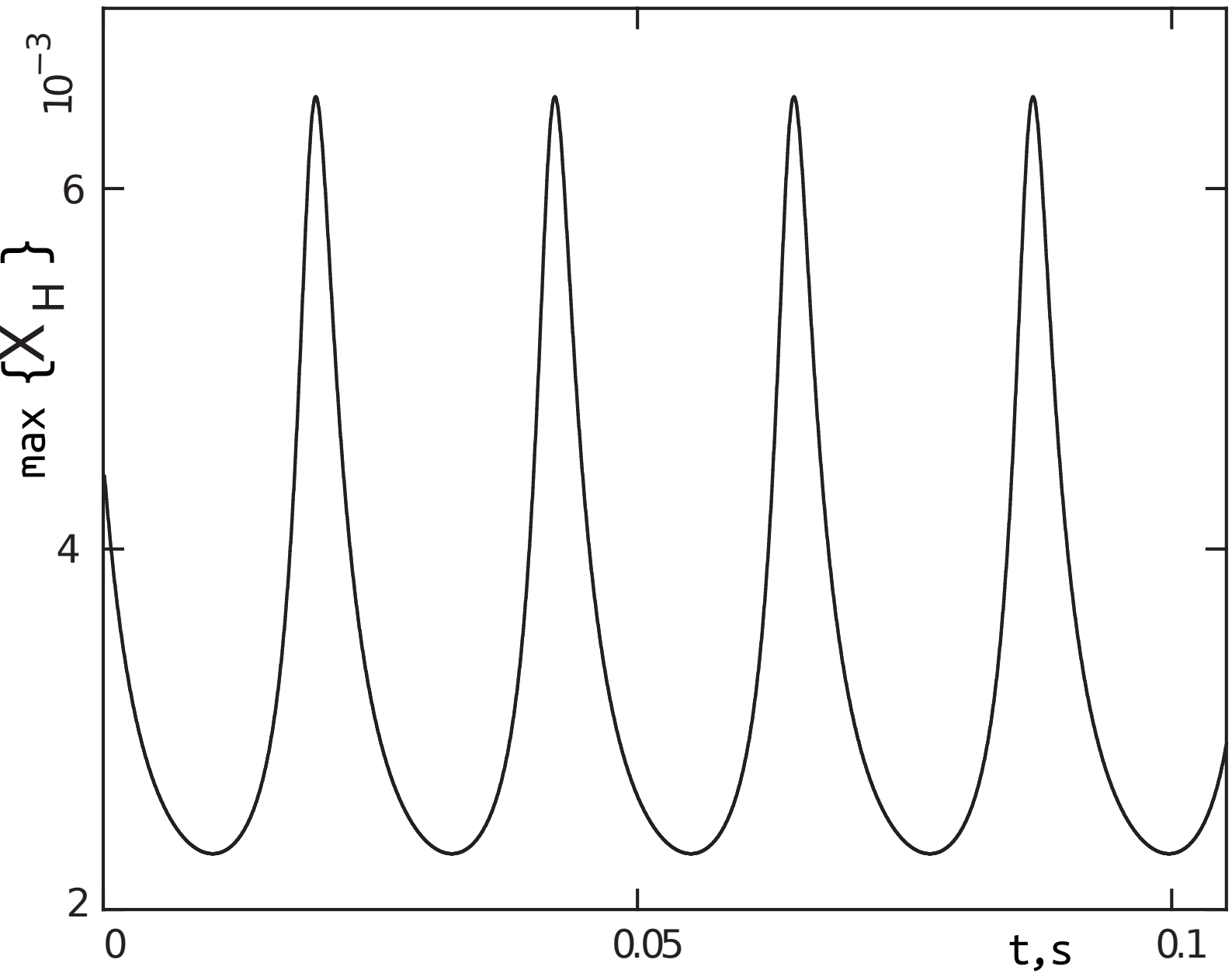

Figure 12

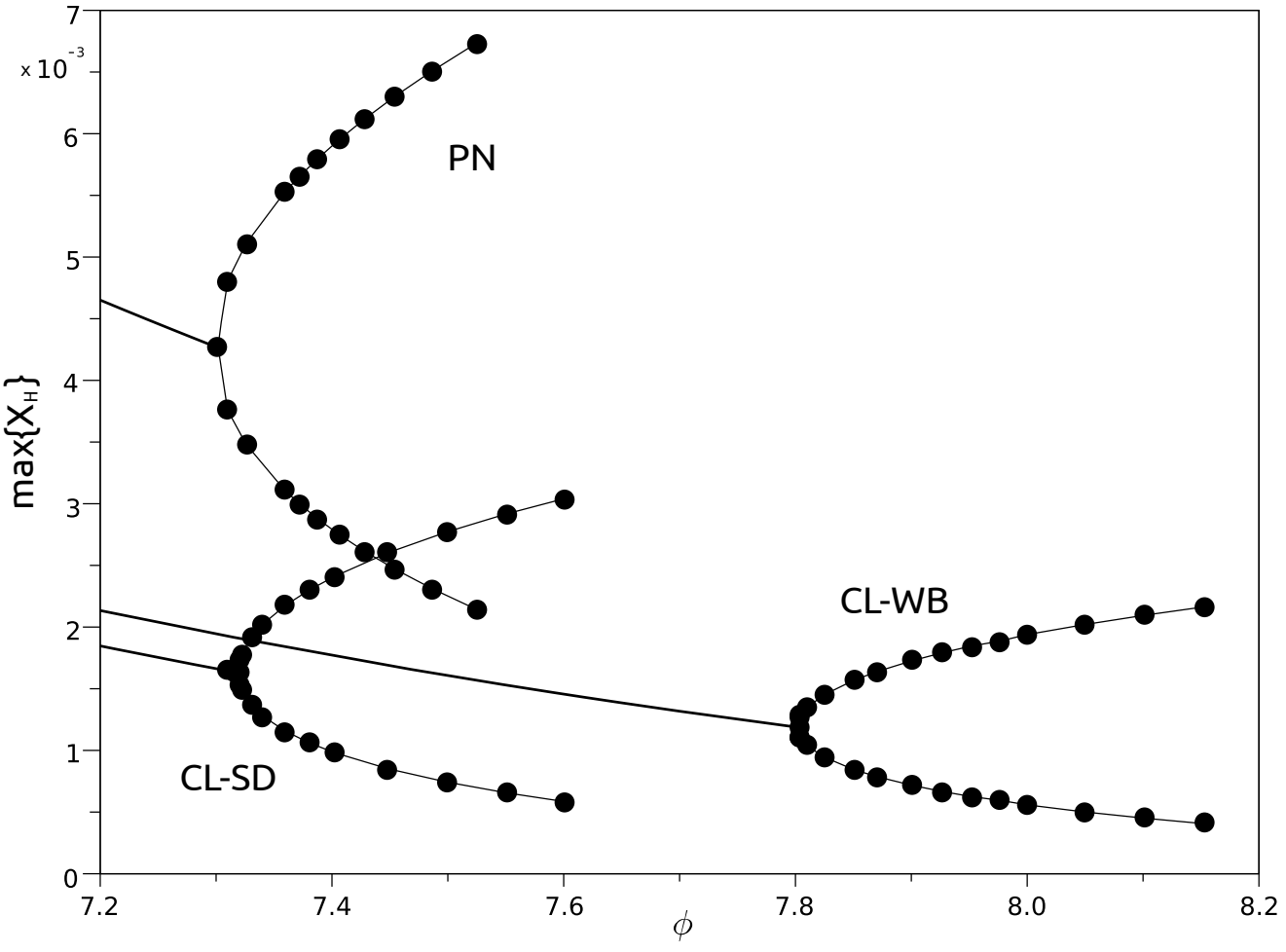

Figure 13

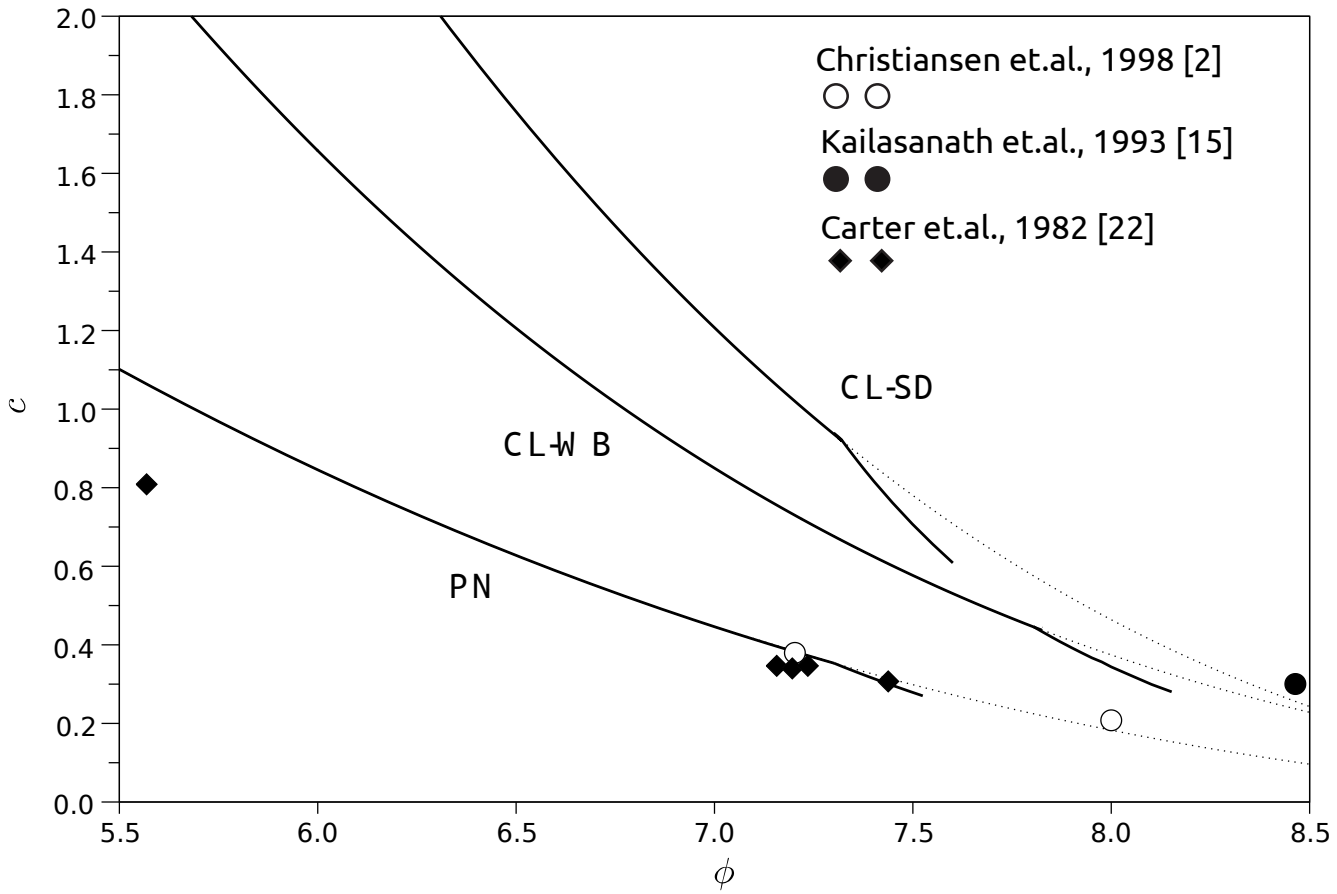
Christiansen et.al., 1998 [2]
Kailasanath et.al., 1993 [15]
Carter et.al., 1982 [22]
CL-SD
CL-W B
PN
c
ϕ
2.0
1.8
1.6
1.4
1.2
1.0
0.8
0.6
0.4
0.2
0.0
5.5
6.0
6.5
7.0
7.5
8.0
8.5